HTLV-1 *pX* gene peaks 7 months after infection, accompanied by an increase in tumor necrosis factor-α levels in the spinal cord and down-regulation of the anti-apoptotic *bcl-2* gene in oligodendrocytes.[17,18] Thus, we reasoned that the most crucial molecular events occurred ~7 months after HTLV-1 infection in our rat model.

The proinflammatory cytokine interferon (IFN)-γ, secreted from activated T and NK cells, increases MHC class I and II expression on a wide variety of cells and then induces a Th1-type immune response. Until recently, IFN-γ had been considered a deleterious factor for central nervous system (CNS) disorders such as multiple sclerosis and experimental autoimmune encephalomyelitis.[19,20] However, several lines of evidence indicate that, in some instances, IFN-γ exerts protective effects against CNS disorders. First, inactivation of the *IFN-γ* gene by gene knockout converts an otherwise experimental autoimmune encephalomyelitis-resistant mouse strain to experimental autoimmune encephalomyelitis-susceptible.[21] Second, a low level of IFN-γ expression in the CNS plays a protective role in cuprizone-induced demyelination.[22] Third, BALB/c mice treated with an anti-IFN-γ antibody become susceptible to measles virus encephalitis, and viral clearance from the CNS is impaired.[23] Fourth, treatment with IFN-γ results in inhibition of viral replication in primary cultured nerve cells infected with measles virus.[24] Fifth, IFN-γ protects neurons from apoptosis during destructive encephalitis induced by herpes simplex virus type 1.[25] In these reports,[21–25] the authors assumed that IFN-γ was derived from mononuclear cells, including T and NK cells, infiltrating into the CNS.

We show here that IFN-γ levels in the spinal cord are significantly increased in HAM-resistant ACI and LEW rats 7 months after HTLV-1 infection, whereas no such increase occurs in HAM-susceptible WKAH rats. Infiltration of mononuclear cells was never seen in the CNS of HTLV-1-infected rats, indicating that IFN-γ was produced by resident cells of the CNS. By confocal laser-scanning microscopy, we identified IFN-γ-producing cells in the spinal cord of HAM-resistant rats as neurons. We suggest that IFN-γ produced by neurons in response to HTLV-1 infection has a protective role against the development of myelopathy.

Materials and Methods

Rats and HTLV-1 Infection

Inbred ACI, LEW, and WKAH rats were obtained from the Institute for Animal Experimentation, Hokkaido University Graduate School of Medicine. HTLV-1 infection was achieved as described.[12] Briefly, HTLV-1-immortalized MT-2[26] was injected into the peritoneal cavity of newborn rats (1×10^7 cells/rat). All HTLV-1-infected rats were maintained in the P3 room. At least three rats were used in each experiment. All rats used in this study were anesthetized with sodium pentobarbital and then intravascularly perfused with ice-cold saline. All animal experiments were done in accordance with the Guide for Care and Use of Laboratory Animals in Hokkaido University Graduate School of Medicine.

Tissue Sampling for mRNA Extraction

After perfusion with ice-cold saline, the spinal cord, cerebrum, and spleen were harvested, flash-frozen in liquid nitrogen, and served as samples for mRNA extraction. Microglia- and neuron-rich populations were prepared from the spinal cord as follows: the harvested spinal cord was dissected and then incubated in RPMI 1640 medium (Sigma-Aldrich, St. Louis, MO) containing 0.25% collagenase (Worthington Biochemical Corp., Freehold, NJ) and 700 U DNase I (Takara, Otsu, Japan) for 30 minutes at 37°C. Microglia-rich populations were separated from the solution by Percoll-gradient centrifugation as described by Tomaru and colleagues[17] and Jiang and colleagues.[18] For separation of neuron-rich populations, myelin residues were removed from the solution by centrifugation at $6 \times g$ for 1 minute, and then neurons in the supernatant were collected by centrifugation at $36 \times g$ for 7 minutes. All samples were stored at −80°C until use.

Reverse Transcriptase-Polymerase Chain Reaction (RT-PCR) and Quantitative Real-Time RT-PCR

Total RNAs were extracted using Isogen (Nippon Gene, Tokyo, Japan) and purified using the RNeasy mini kit (Qiagen, Alameda, CA). The purified total RNAs were reverse-transcribed using the Super Script III first-strand synthesis system for RT-PCR (Invitrogen, Carlsbad, CA). Quantitative real-time RT-PCR was done with the cDNAs, SYBR Green I dye (SYBR Green PCR Master Mix; Qiagen), and the primer set for *IFN-γ* (sense: 5′-GATCCAGCACAAAGCTGTCA-3′, anti-sense: 5′-GACTCCTTTTCCGCTTCCTT-3′), *interferon regulatory factor 1* (*IRF-1*) (sense: 5′-TGAAGCTGCAACAGATGAGG-3′, anti-sense: 5′-AGCAAGTATCCCTTGCCATC-3′), *IL-12p40* (sense: 5′-AGGTGCGTTCCTCGTAGAGA-3′, anti-sense: 5′-CCATTTGCTGCATGATGAAT-3′), *IL-12 receptor β1* (*IL-12Rβ1*) (sense: 5′-AGGTGCAGATTTCCCGTTTA-3′, anti-sense: 5′-CAGCCCTGTTTAAGCCAATG-3′), *IL-12 receptor β2* (*IL-12Rβ2*) (sense: 5′-TGCCACCAATCCACAAACTA-3′, anti-sense: 5′-CCTGCTTCCTAGCACCTTGT-3′), *IL-23p19* (sense: 5′-CACCACTGGGAGACTCAACA-3′, anti-sense: 5′-AGGATCTTGGAACGGAGAAGA-3′), *IL-23 receptor* (*IL-23R*) (sense: 5′-TTGATGAATTGTGCCTCGTT-3′, anti-sense: 5′-GTCTGCGCTGGGATAGTTTC-3′), *IL-27* (sense: 5′-ACTCTGCTTCCTCGCTACCA-3′, anti-sense: 5′-GGAGATCCAGCCTCATTGC-3′), *IL-27 receptor* (*IL-27R, WSX-1*) (sense: 5′-AGCCCAGGGATAAAGGTGAC-3′, anti-sense: 5′-AGACGGGTCCAGTTGAGCTT-3′), or *GAPDH* (sense: 5′-ATGGGAGTTGCTGTTGAAGTCA-3′, anti-sense: 5′-CCGAGGGCCCACTAAAGG-3′). PCR was performed in a two-step reaction (95°C for 30 seconds, 60°C for 30 seconds) for 45 cycles after initial denaturation (95°C, 15 minutes), using the ABI Prism 7000 sequence detector

system (Applied Biosystems, Foster City, CA). Relative expression of target genes was analyzed using the ΔΔCT-method.[27] The amount of specific mRNA was quantified at the point where the system detected uptake in the exponential phase of PCR accumulation and normalized to *GAPDH* mRNA levels.

Emzyme-Linked Immunosorbent Assay (ELISA)

ELISA for rat IFN-γ was performed using a kit (BioSource, Camarillo, CA). In brief, after perfusion with ice-cold saline, harvested spinal cords were homogenized with 1 ml of phosphate-buffered saline (PBS) containing 10 μg/ml aprotinin, 1 μg/ml leupeptin, and 1 μg/ml phenylmethyl sulfonyl fluoride. Duplicate samples (100 μl) of spinal cord homogenates were subjected to ELISA according to the manufacturer's instructions. The detection limit of the kit was 13 pg/ml.

Primary Culture of Rat Spinal Cord Cells

Saline-perfused spinal cords were obtained from rats 7 months after HTLV-1 infection and from age-matched control rats. Harvested spinal cords were dissected and digested as described above. Cell suspensions were centrifuged, and then the pellet was resuspended in 30% Percoll (Amersham Biosciences, Uppsala, Sweden) diluted with Hanks' balanced salt solution (Invitrogen, Carlsbad, CA). The cell suspension was laid gently on 80% Percoll solution. The gradient solution was centrifuged at 1800 × *g* for 40 minutes. Cells in the 30% Percoll layer were dissociated, washed, and then plated sparsely on poly-L-lysine-coated dishes in Dulbecco's modified Eagle's medium/Ham's F12 medium (Invitrogen) supplemented with 10% fetal calf serum and 50 ng/ml of nerve growth factor 2.5S (Invitrogen) at 37°C in an atmosphere of 5% CO_2.

Recombinant Cytokines

Recombinant rat IFN-γ was purchased from PeproTech EC (London, UK). Recombinant mouse interleukin (IL)-12, previously shown to function in rats,[28] was purchased from R&D Systems (Minneapolis, MN).

Immunofluorescent Staining

Cells cultured on poly-L-lysine/laminin-coated glasses for 5 days were fixed with 4% paraformaldehyde for 15 minutes. For intracellular staining, cells were treated with PBS containing 0.1% Triton-X and 0.05% bovine serum albumin for 4 minutes and then fixed with ice-cold 70% methanol for 4 minutes. Nonspecific binding was blocked with PBT (0.05% Tween-20/0.1% bovine serum albumin in PBS) containing 0.1% goat serum for 10 minutes. Primary antibodies used were mouse monoclonal anti-rat IFN-γ (DB1; PBL Biomedical Laboratories, Piscataway, NJ), mouse monoclonal anti-rat CD68 (ED-1; Serotec, Oxford, UK), rabbit polyclonal anti-neurofilament (NF) 150-kd molecule (AB1981; Chemicon International, Temecula, CA), and rabbit polyclonal anti-glial fibrillary acidic protein (GFAP) (Dakocytomation, Glostrup, Denmark). For double staining, cells were labeled with DB1 and AB1981, DB1 and anti-GFAP, or ED-1 and AB1981 followed by labeling with Alexa Fluor 488-conjugated goat polyclonal antibody to mouse IgG and Alexa Fluor 568-conjugated goat polyclonal antibody to rabbit IgG. Confocal images were acquired with a laser-scanning microscope (MRC-1024; Bio-Rad Laboratories, Hercules, CA).

Effects of IFN-γ on HTLV-1 Gene Expression

LEW-S1,[12] an HTLV-1-immortalized rat T-cell line, was incubated with 100 or 1000 U/ml recombinant rat IFN-γ for 3 hours, and the relative expression of the HTLV-1 *pX* gene to the structural *gag* gene was calculated using the quantitative real-time RT-PCR method. Primer sets used were 5′-ATCCCGTGGAGACTCCTCAA-3′ (sense) and 5′-CCAAACACGTAGACTGGGTATCC-3′ (anti-sense) for *pX* and 5′-CCAATGCAAACAAAGAATGC-3′ (sense) and 5′-AGCCCGCAACATATCTCCTA-3′ (anti-sense) for *gag*.

Sequencing of the 5′-Flanking Region of the Rat IL-12Rβ2 Gene

Genomic DNA was extracted from the tails of ACI, LEW, and WKAH rats using the DNeasy tissue kit (Qiagen). The 5′-flanking region of the *IL-12Rβ2* gene (1.8 kb) was amplified by nested PCR (outer primers, 5′-ACCACACCTCTTGCCATTTT-3′ and 5′-CGAATCGGAGTACACTGCTG-3′; inner primers, 5′-CCCAGAGGCACTTTAAGCA-3′ and 5′-ACCGATGGACAATGGGTATC-3′). After gel electrophoresis, the PCR products were purified with Freeze 'N Squeeze DNA gel extraction spin columns (Bio-Rad Laboratories) and subjected to direct sequencing with the CEQ 2000XL DNA analysis system (Beckman-Coulter, Fullerton, CA). Sequences were aligned using the online ClustalW service (*http://www.ddbj.nig.ac.jp/search/clustalw-j.html*) and potential binding sites of transcription factors were identified using the Transfec database (*http://motif.genome.jp/*).

Statistical Analysis

Data were analyzed with either Student's *t*-test or repeated measures analysis of variance, appropriately. *P* values less than 0.05 were considered to be significant.

Results

HTLV-1 Infection Induces IFN-γ Production in the Spinal Cord of HAM-Resistant but Not HAM-Susceptible Rats

In view of the fact that IFN-γ exerts protective effects against CNS disease,[21–25] we compared the expres-

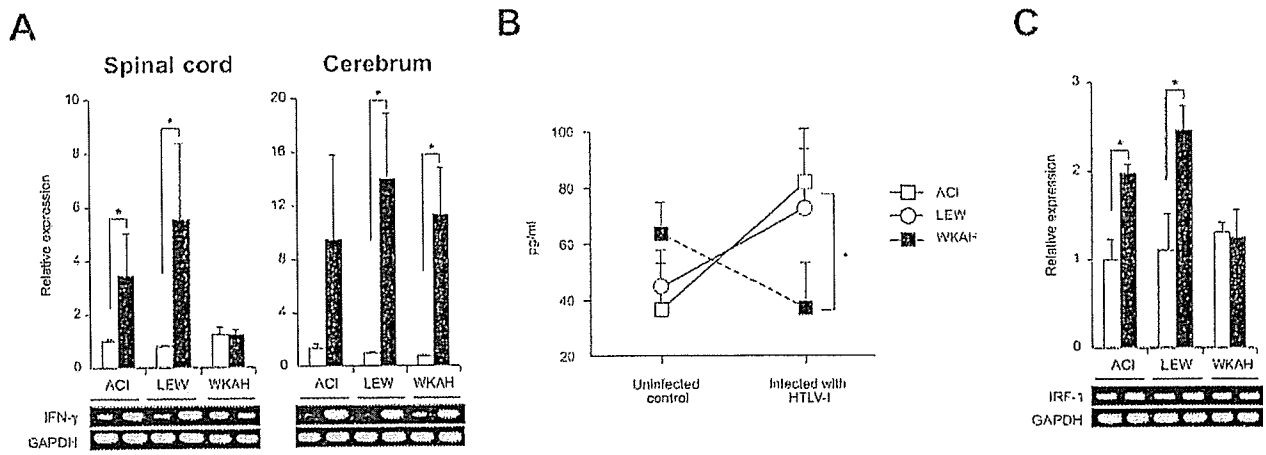

Figure 1. **A:** The amount of *IFN-γ* mRNA in the spinal cord and cerebrum was quantified by real-time RT-PCR. Samples were obtained from rats 7 months after HTLV-1 infection (**black columns**) and from age-matched uninfected controls (**white columns**). Results of experiments done in triplicate were evaluated as relative expression levels to the *GAPDH* gene. Data are represented as mean ± SD values of experiments done independently three times. Representative photos of gel electrophoresis of RT-PCR products are shown beneath the graph. **B:** The amount of IFN-γ protein in the spinal cord was quantified using the ELISA kit. Samples were obtained from rats 7 months after HTLV-1 infection and from age-matched uninfected controls. Data are represented as mean ± SD values of experiments done independently three times. **C:** The amount of *IRF-1* mRNA in the spinal cord was quantified by real-time RT-PCR. Samples were obtained from rats 7 months after HTLV-1 infection (**black columns**) and from age-matched uninfected controls (**white columns**). Results of experiments done in triplicate were evaluated as relative expression levels to the *GAPDH* gene. Data are represented as mean ± SD values of experiments done independently three times. Representative photos of gel electrophoresis of RT-PCR products are shown beneath the graph. In each group of all experiments, at least three rats were used. $^{*}P < 0.05$.

sion levels of *IFN-γ* mRNA between HAM-susceptible and -resistant rats 7 months after inoculation with HTLV-1 (Figure 1). Expression of *IFN-γ* was quantified by real-time RT-PCR in the spinal cord, cerebrum, and spleen. We used tissue samples obtained 7 months after infection because our previous work indicated that critical molecular events leading to the development of HAM rat disease occurred at this time period.[17,18,29]

The expression of *IFN-γ* in the spinal cord, an organ affected in HAM rat disease, was significantly elevated in HAM-resistant ACI and LEW rats compared with age-matched, uninfected controls, whereas the expression levels of *IFN-γ* in the spinal cord of HAM-susceptible WKAH rats were almost the same as those in uninfected controls (Figure 1A, left). The expression of *IFN-γ* in the cerebrum, an organ never affected in HAM rat disease, was remarkably increased in infected rats regardless of whether they were HAM-resistant or -susceptible (Figure 1A, right). In spleen cells, the mRNA level of *IFN-γ* did not change by infection; however, even in the absence of infection, *IFN-γ* was expressed more abundantly than in the cerebrum of infected rats (data not shown). Increased expression of *IFN-γ* mRNA was not evident in the spinal cord of HAM-resistant rats 3 months after infection, when the provirus was barely detected (data not shown).

To evaluate expression of IFN-γ at the protein level, spinal cords were harvested from infected and age-matched uninfected rats and the tissue extracts subjected to assay using an ELISA kit. Consistent with the results obtained at the mRNA level, the amount of IFN-γ proteins in the spinal cord was increased in HAM-resistant ACI and LEW rats but not in HAM-susceptible WKAH rats when measured 7 months after HTLV-1 infection (Figure 1B).

We next examined expression of the *IRF-1* gene. IRF-1 is known as a downstream molecule induced by IFN-γ.[30] Like IFN-γ, expression of *IRF-1* was significantly increased in the spinal cord of ACI and LEW rats 7 months after infection, whereas no such increase was seen in the spinal cord of WKAH rats (Figure 1C). Thus, collective evidence clearly indicated that IFN-γ was induced by HTLV-1 infection only in the spinal cords of HAM-resistant strains.

IFN-γ Suppresses pX Gene Expression in Cultured HTLV-1-Immortalized Rat Cells

IFN-γ was recently shown to have a negative regulatory role against HTLV-1 gene expression.[31] To examine whether IFN-γ can suppress expression of the *pX* gene, previously shown to play a critical role in the

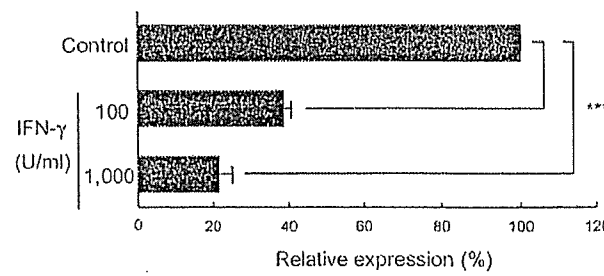

Figure 2. The HTLV-1-immortalized rat T-cell line, LEW-S1, was incubated with 100 or 1000 U/ml of recombinant rat IFN-γ for 3 hours, and then expression of the *pX* gene was quantified using the real-time RT-PCR method. Results of experiments done in triplicate were evaluated as relative expression levels to the structural *gag* gene. Data are represented as mean ± SD values of experiments done independently three times. $^{***}P < 0.0001$.

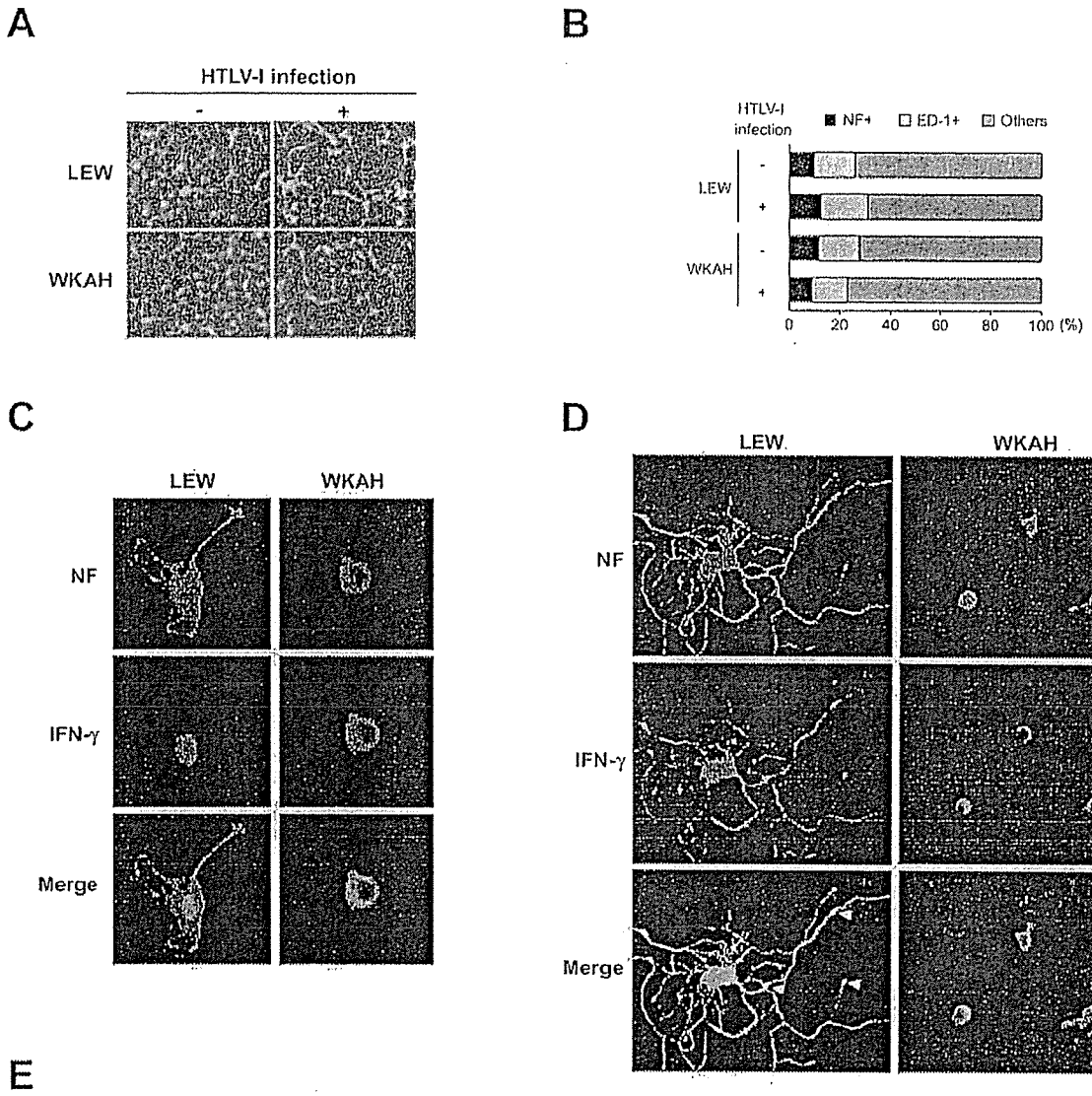

Figure 3. Spinal cord cells were isolated from HTLV-1-infected rats and from age-matched uninfected rats. Infected rats were sacrificed 7 months after inoculation with HTLV-1. **A:** Phase-contrast photos of cultured cells. **B:** Cells cultured on poly-L-lysine/laminin-coated glasses for 5 days were fixed and then used for double-immunofluorescent staining for NF (a marker for neurons) and ED-1 (a marker for microglia). The proportion of each cell population in the culture was calculated. **C** and **D:** Spinal cord cells derived from uninfected (**C**) and HTLV-1-infected rats (**D**) were stained for NF (red) and IFN-γ (green). **Arrowheads** indicate the expression of IFN-γ in synapses. **E:** Ratios of IFN-γ^+ cells in neurons (NF^+ cells) and astrocytes ($GFAP^+$ cells) in the spinal cord. Cells were isolated from the spinal cord of rats 7 months after HTLV-1 infection (**black columns**) and from age-matched uninfected controls (**white columns**). After double staining for IFN-γ and NF, or IFN-γ and GFAP, 100 cells were counted in three independent high-power views, respectively, under a fluorescence microscope. In each group, at least three rats were used. Results are represented as mean ± SD values of experiments done independently three times. $^{**}P < 0.001$. Original magnifications: ×200 (**A**); ×620 (**C**, **D**).

onset of HAM rat disease,[17,18] we treated the HTLV-1-immortalized rat T-cell line LEW-S1[12] with IFN-γ for 3 hours *in vitro* and then monitored expression of the *pX* gene by real-time RT-PCR (Figure 2). Expression of the *pX* gene relative to that of the structural *gag* gene was decreased in response to IFN-γ in a dose-dependent manner. These results suggest that IFN-γ is likely to protect against the development of HAM rat disease by down-regulating *pX* gene expression. Thus, WKAH rats presumably develop HAM rat disease because their spinal cord cells cannot produce IFN-γ in response to HTLV-1 infection.

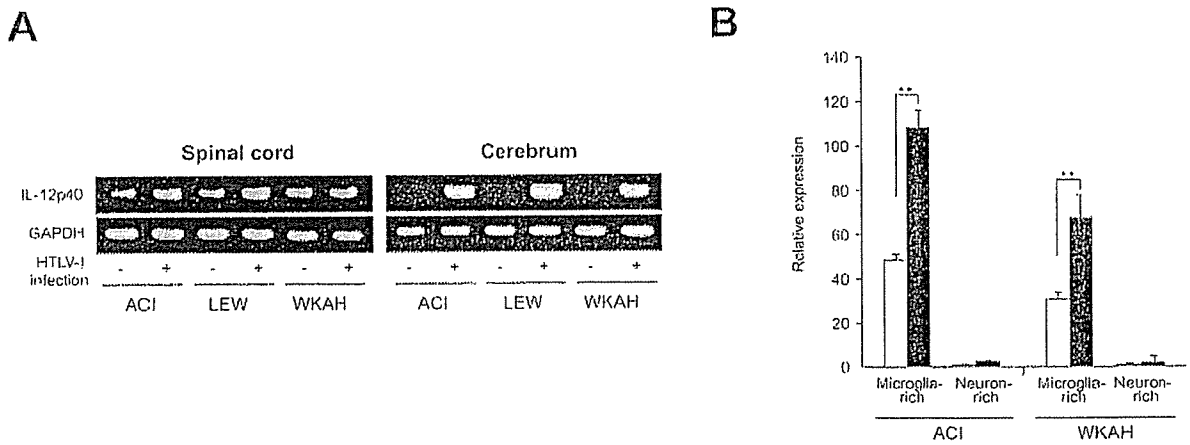

Figure 4. **A:** Expression of the *IL-12p40* gene in the spinal cord and cerebrum. Samples were obtained from rats 7 months after HTLV-1 infection and from age-matched uninfected controls. Experiments were repeated independently at least three times. Representative photos of gel electrophoresis of RT-PCR products are shown. **B:** The amount of *IL-12p40* mRNA in microglia- or neuron-rich populations prepared from the spinal cord was quantified by real-time RT-PCR. Samples were obtained from rats 7 months after HTLV-1 infection (**black columns**) and from age-matched uninfected controls (**white columns**). Data (relative expression levels to the *GAPDH* gene) are represented as mean ± SE values obtained from experiments performed in triplicate and repeated three times. In each group, at least three rats were used. $^{**}P < 0.001$.

Cells that Produce IFN-γ in the Spinal Cord of HTLV-1-Infected HAM-Resistant Rats Are Neurons

To identify IFN-γ-producing cells, we established primary cultures of rat spinal cord cells from both LEW and WKAH strains (Figure 3A). These cells were observed under a confocal laser-scanning microscope after immunofluorescent double staining for NF and ED-1. The cultured cells prepared from both strains, infected and uninfected, contained a nearly equivalent proportion of NF^+ neurons, ED-1^+ microglia, and other glial cells (Figure 3B), thus ensuring that the samples subjected to comparison were not substantially different in terms of cell populations.

We stained the cells with antibodies for NF and IFN-γ, or for GFAP and IFN-γ, and focused our analysis on neurons and astrocytes because they are known to express IFN-γ in the CNS.[32–34] Weak expression of IFN-γ was seen in the perinuclear cytoplasm of NF^+ neurons derived from uninfected LEW and WKAH rats (Figure 3C). The neurons obtained from LEW rats infected with HTLV-1 showed intense immunoreactivity to IFN-γ not only in the perinuclear cytoplasm but also in the dendrites, whereas HTLV-1 infection did not cause any significant alteration in the staining pattern or morphology in the neurons of WKAH rats as compared with those of uninfected control rats (Figure 3D). Neurite outgrowth was markedly induced by HTLV-1 infection in LEW but not WKAH rats. IFN-γ treatment is known to induce differentiation of neurons and an outgrowth of dendrites.[35] Thus, the morphological alterations seen in Figure 3, C and D, are consistent with the observation that HTLV-1 infection induced IFN-γ expression in the spinal cord of HAM-resistant but not HAM-susceptible rats (Figure 1). We presume that IFN-γ produced by neurons of LEW rats acts in an autocrine and/or paracrine manner and promotes their differentiation and neurite outgrowth. Interestingly, IFN-γ induced in the neurons of HTLV-1-infected LEW rats appeared to accumulate in synaptic junctions (Figure 3D, arrowheads). This is in line with the observation that the receptors for IFN-γ are expressed at synapses in the superficial dorsal horn and lateral spinal nucleus[36] and suggests that IFN-γ produced in neurons might function as a neurotransmitter in the CNS. On the other hand, the expression of IFN-γ in $GFAP^+$ astrocytes was weak regardless of whether they originated from infected or uninfected animals or from HAM-susceptible or -resistant strains (data not shown). Quantitative analysis based on cell counting confirmed that neurons rather than astrocytes were the major IFN-γ-producing cells in the spinal cord of infected rats (Figure 3E).

Spinal Cord Cells of HAM-Susceptible Rats Do Not Produce IFN-γ in Response to IL-12

Certain infections induce production of IL-12, which in turn promotes production of IFN-γ.[37] Our RT-PCR experiments showed that HTLV-1 infection induced expression of *IL-12p40* mRNA in the cerebrum of both HAM-resistant and -susceptible strains (Figure 4A, right). Induction of *IL-12p40* was not obvious when the whole spinal cord samples were subjected to analysis (Figure 4A, left); however, when they were fractionated into microglia- and neuron-rich populations, we could clearly see elevated expression of *IL-12p40* in the former, but not in the latter, populations (Figure 4B). These findings are consistent with our previous observation that the HTLV-1 provirus was localized to microglia and macrophages.[16] Basal *IL-12p40* mRNA levels in the microglia-rich population were lower in WKAH than in ACI rats. However, in both strains, HTLV-1 infection almost doubled the expression levels of *IL-12p40* in microglia-rich populations (Figure 4B). We thus reasoned that the failure of WKAH spinal cord cells to produce IFN-γ is unlikely to be caused by defective induction of IL-12.

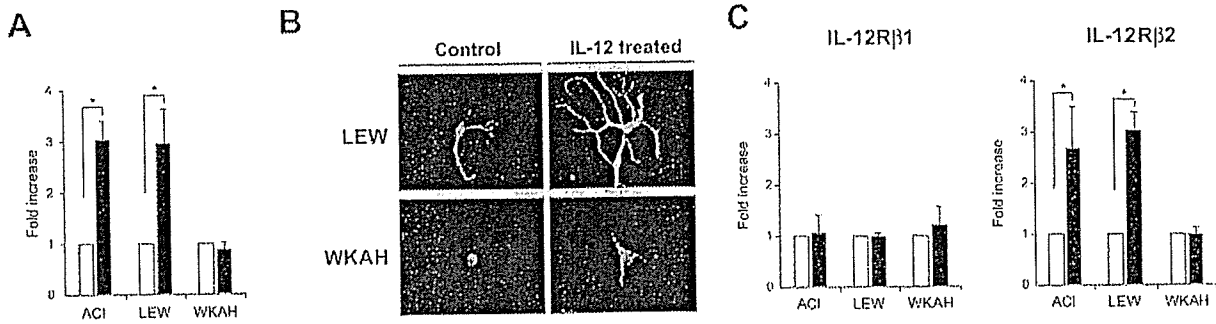

Figure 5. **A:** The amount of *IFN-γ* mRNA in the cells isolated from the spinal cord of uninfected rats was quantified by real-time RT-PCR. Samples were obtained from the cells after treatment with recombinant IL-12 (100 ng/ml) for 18 hours (**black columns**). Results of experiments done in triplicate and repeated three times were evaluated as mean ± SE values of the fold increase to the data without IL-12 treatment (**white columns**). $^*P < 0.05$. **B:** Cells isolated from the spinal cord of uninfected rats were cultured on poly-L-lysine/laminin-coated glasses. After incubation with recombinant IL-12 (100 ng/ml) for 5 days, immunofluorescent double staining was performed using anti-IFN-γ (green) and anti-NF (red) antibodies. Representative merged images are shown. Experiments were performed independently three times. **C:** The amount of *IL-12Rβ1* and *IL-12Rβ2* mRNAs in the cells isolated from the spinal cord of uninfected rats was quantified by real-time RT-PCR. Samples were obtained from the cells after treatment with recombinant IL-12 (100 ng/ml) for 18 hours (**black columns**). Results of experiments done in triplicate and repeated three times were evaluated as mean ± SE values of the fold increase to the data without IL-12 treatment (**white columns**). $^*P < 0.05$. For all experiments, at least three rats were used in each group. Original magnifications, ×620 (**B**).

We then tested the possibility that the inability of WKAH rats to produce IFN-γ in their spinal cords is caused by defective response to IL-12. To this end, primary culture cells from the spinal cord of uninfected rats were treated with IL-12 *in vitro*, and then expression of *IFN-γ* was examined. By exposure to IL-12 for 18 hours, expression levels of *IFN-γ* were markedly increased in tissue-cultured spinal cord cells from HAM-resistant ACI and LEW rats, whereas no alteration was seen in the cells from HAM-susceptible WKAH rats (Figure 5A).

We confirmed by immunofluorescent staining that treatment with IL-12 induced IFN-γ only in the neurons of HAM-resistant rats (Figure 5B). IL-12 also induced neurite outgrowth in neurons prepared from LEW rats, presumably through the actions of IFN-γ. By contrast, similar treatment did not induce neurite outgrowth in WKAH rats. Thus, the unresponsiveness of WKAH-derived neurons to IL-12 *in vitro* closely mirrored the inability of WKAH-derived neurons to produce IFN-γ and undergo neurite outgrowth in response to HTLV-1 infection (Figures 1 and 3).

Spinal Cord Cells from HAM-Susceptible Rats Do Not Show Elevated IL-12Rβ2 Expression in Response to IL-12

To understand why WKAH neurons do not respond to IL-12, we examined expression of IL-12 receptors in tissue-cultured spinal cord cells obtained from HAM-resistant and -susceptible strains. IL-12 receptors are composed of β1 and β2 subunits.[38] Although *IL-12Rβ1* is expressed constitutively, expression of *IL-12Rβ2* is up-regulated by IL-12. Expression levels of *IL-12Rβ1* mRNA were not altered by IL-12 treatment in HAM-resistant or -susceptible strains (Figure 5C, left). By contrast, treatment with IL-12 markedly increased *IL-12Rβ2* mRNA in spinal cord cells from ACI and LEW but not from WKAH rats (Figure 5C, right). These results indicate that the absence of IFN-γ production in the spinal cord of WKAH rats results from the inability of the *IL-12Rβ2* gene to respond to IL-12 signals.

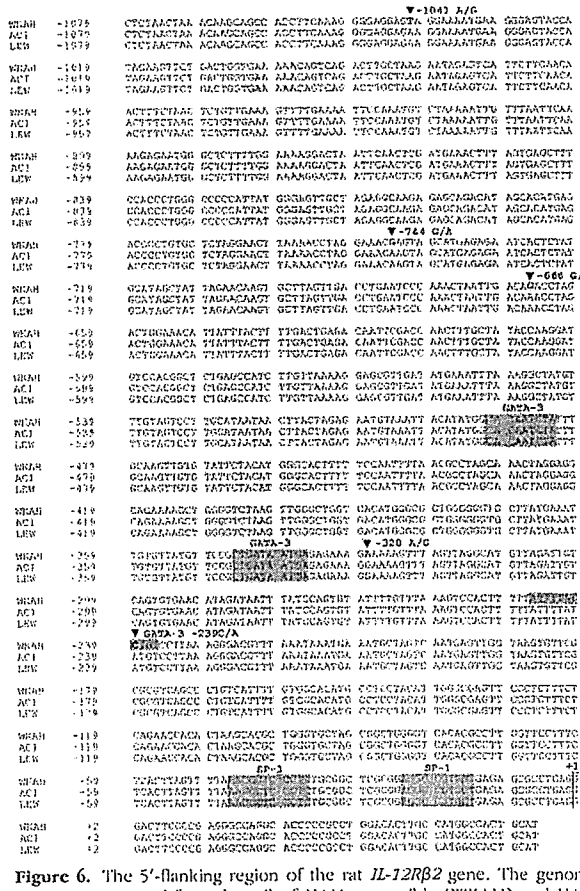

Figure 6. The 5′-flanking region of the rat *IL-12Rβ2* gene. The genomic DNA was extracted from the tail of HAM-susceptible (WKAH) and HAM-resistant (ACI, LEW) rats, and then the 5′-flanking region of the *IL-12Rβ2* gene was amplified by nested PCR. The PCR products were purified and subjected to direct sequencing. **Shaded** sequences represent potential SP-1 or GATA-3 binding sites. +1 represents a tentatively assigned transcription start site deduced from the data available for the mouse *IL-12Rβ2* gene.

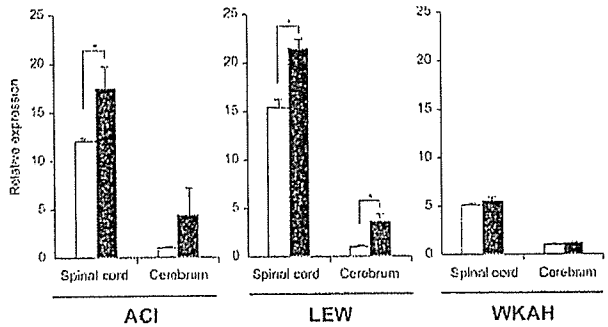

Figure 7. The amount of *IL-12Rβ2* mRNA in the spinal cord and cerebrum was quantified by real-time RT-PCR. Samples were obtained from rats 7 months after HTLV-1 infection (**black columns**) and from age-matched uninfected controls (**white columns**). Results of experiments performed in triplicate were evaluated as relative expression levels to the *GAPDH* gene. For each strain, the expression level of *IL-12Rβ2* mRNA in the cerebrum of uninfected control rats was set as 1. Relative expression levels (mean ± SD values) were determined from the experiments done independently three times. In each group, at least three rats were used. $^{*}P < 0.05$.

The 5′-Flanking Region of the Rat IL-12Rβ2 Gene Is Polymorphic

To examine whether the defect is in the *IL-12Rβ2* gene itself, we compared its 5′-flanking sequence between HAM-resistant and -susceptible strains. Although HAM-resistant ACI and LEW rats had an identical sequence, the sequence of HAM-susceptible WKAH rats differed from that of ACI and LEW rats by 5 bp in the region spanning −1079 to −1 (Figure 6). We focused our analysis on SP-1 and GATA-3 binding sites because expression of the *IL-12Rβ2* gene has been shown to be regulated positively and negatively by SP-1 and GATA-3 transcription factors, respectively.[39,40] None of the 5-bp substitutions affects potential SP-1 binding sites; however, the substitution from A to C at nucleotide position −239 generates an additional potential GATA-3 binding site in the WKAH sequence. As a result, there are three potential GATA-3 binding sites in WKAH, whereas ACI and LEW have only two such sites. Because GATA-3 is known to repress *IL-12Rβ2* gene expression strongly,[40] the single nucleotide polymorphism at nucleotide position −239 may be related to the defective induction of *IL-12Rβ2* transcription in WKAH rats.

In HAM-Susceptible Rats, HTLV-1 Infection Elevates mRNA Expression of IL-23, IL-27, and Their Receptors in the Cerebrum but Not in the Spinal Cord

In line with the *in vitro* studies, HTLV-1 infection did not induce *IL-12Rβ2* mRNA in the spinal cord or the cerebrum in WKAH rats (Figure 7). By contrast, HTLV-1 infection elevated *IL-12Rβ2* mRNA in both the spinal cord and cerebrum in HAM-resistant ACI and LEW rats. In WKAH rats, defective induction of *IL-12Rβ2* mRNA was observed not only in the spinal cord, but also in the cerebrum (Figure 7). This raised the question of why IFN-γ was induced in the cerebrum of WKAH rats 7 months after HTLV-1 infection (Figure 1A). To answer this question, we focused our analysis on IL-23 and IL-27 because these cytokines are known to induce IFN-γ.[41] IL-23 is composed of p19 and p40 subunits,[42] and the p40 subunit is shared by IL-12. IL-23 receptors are made up of IL-12Rβ1 and the specific subunit, IL-23R. Expression levels of *IL-23p19*, *IL-12Rβ1*, *IL-23R*, *IL-27*, and *IL-27R* (*WSX-1*) genes were significantly increased in the cerebrum but not in the spinal cord of WKAH rats 7 months after HTLV-1 infection (Figure 8). These observations indicate that IFN-γ was induced in the cerebrum of WKAH rats through the IL-23 and/or IL-27 pathways.

Discussion

In the present study, we have demonstrated that expression of the proinflammatory cytokine IFN-γ is significantly elevated in the spinal cord of HAM-resistant rats 7 months after HTLV-1 infection (Figure 1). The increased expression of IFN-γ in the spinal cord was seen only in HAM-resistant strains. Importantly, we found that IFN-γ could suppress expression of the *pX* gene *in vitro* (Figure 2), the gene previously shown to be critically involved in the development of myelopathy in WKAH rats.[17,18] Thus, combined evidence argues strongly that IFN-γ prevents the development of myelopathy by down-regulating *pX* gene expression in the spinal cord. However, there may be other mechanisms through which IFN-γ exerts protective effects against HAM rat disease. For example, IFN-γ is known to protect cord blood mononuclear cells from HTLV-1 infection when they are co-cultured with an

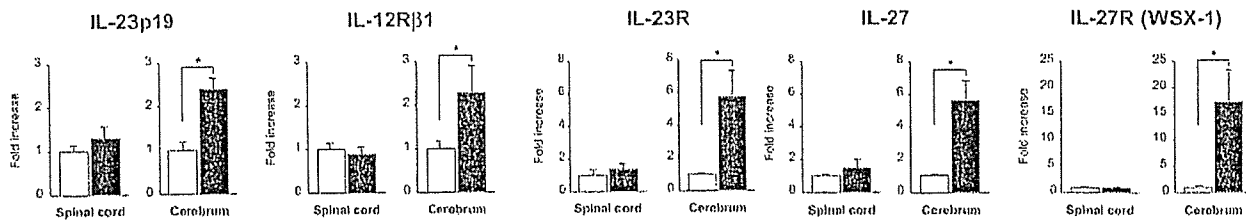

Figure 8. The amounts of *IL-23p19*, *IL-12Rβ1*, *IL-23R*, *IL-27*, and *IL-27R* (*WSX-1*) mRNAs in the spinal cord and cerebrum were quantified by real-time RT-PCR. Samples were obtained from WKAH rats 7 months after HTLV-1 infection (**black columns**) and from age-matched uninfected controls (**white columns**). In each group, at least three rats were used. Results of experiments done in triplicate were evaluated as relative expression levels to the *GAPDH* gene. Data from experiments done independently three times are represented as the fold increase (mean ± SD values) to the data without infection (**white columns**). $^{*}P < 0.05$.

HTLV-1-immortalized T-cell line MT-2, without altering the provirus load in the culture.[31] Thus, IFN-γ may protect against the development of myelopathy through multiple mechanisms.

The CNS including the spinal cord has been considered as an absolute immunologically privileged site because of multiple anatomical and biochemical barriers known as blood-brain barriers. However, throughout the past decade, this view has been challenged by a number of observations showing that resident cells of the CNS produce cytokines and that such cytokines affect both proliferation and differentiation of cells in the CNS even under physiological conditions.[43] In the 1990s, it was suggested that endogenous IFN-γ exists in the CNS.[44] Endogenous IFN-γ was detected in the CNS of mice infected with Theiler's virus,[45] and Kiefer and colleagues[46] showed that IFN-γ was produced by rat neurons. Because there was no inflammatory cell infiltration in the CNS of HTLV-1-infected rats, our present study makes a strong case for the production of cytokines by CNS-resident cells. Neurons are not the sole source of IFN-γ in the CNS. Astrocytes in primary culture are known to produce and release IFN-γ after the mechanical and ischemic injuries.[47] It is also known that cultured rat astrocytes secrete IFN-γ in response to tumor necrosis factor-α in a dose-dependent manner.[48] We therefore asked which population of cells produced IFN-γ in the CNS of HTLV-1-infected, HAM-resistant rats. The observation made under a confocal microscope provided convincing evidence that neurons were the major cells that produced IFN-γ in our rat model of myelopathy (Figure 3). This is the first report demonstrating that HTLV-1 infection induces production of IFN-γ by neurons.

To understand why HTLV-1 infection failed to induce production of neuronal IFN-γ in the spinal cord of WKAH rats (Figures 1 and 3), we initially turned our attention to IL-12, an innate cytokine induced early during certain viral infections and a potent stimulator of IFN-γ.[37] This cytokine is secreted mainly from microglia in the CNS,[49] and in HTLV-1-infected rats, the provirus is predominantly localized in microglia and macrophages.[16] We therefore assumed that infected microglia and/or macrophages in the CNS were the most likely source of IL-12. Consistent with this assumption, we detected *IL-12p40* mRNA in microglia-rich populations (Figure 4B). To examine whether poor induction of IL-12 after infection is responsible for the failure of WKAH rats to produce IFN-γ in their spinal cord neurons, we compared induction kinetics of *IL-12p40* mRNA between HAM-resistant and -susceptible strains (Figure 4B). In both ACI and WKAH strains, HTLV-1 infection elevated the amount of *IL-12p40* mRNA almost twofold in the microglia-rich population. Thus, the ability to produce IL-12 in response to infection is apparently not impaired in WKAH rats.

We then examined the possibility that WKAH rats might have a defect in its ability to respond to IL-12. To this end, cultured spinal cord cells from uninfected rats were treated with IL-12 *in vitro*, and then expression of *IFN-γ* was evaluated by real-time RT-PCR and by immunofluorescent staining (Figure 5). These experiments showed that IFN-γ induction by IL-12 occurs only in neurons obtained from the spinal cords of HAM-resistant strains (Figure 5), indicating that signaling through the IL-12 receptor is defective in WKAH.

To examine whether the defect lies in the *IL-12Rβ2* gene itself, we compared its 5′-flanking sequence between HAM-resistant and -susceptible strains. The two HAM-resistant strains, ACI and LEW, had an identical sequence; however, the sequence of WKAH rats differed from that of ACI and LEW by 5 bp (Figure 6). Interestingly, the A to C substitution at nucleotide position −239 generates an additional potential GATA-3 binding site in WKAH rats. Although the mechanism regulating the expression of the *IL-12Rβ2* gene is only poorly understood, GATA-3 is known to repress its expression strongly.[40] Thus, the single nucleotide polymorphism at nucleotide position −239 may be involved in the defective induction of the *IL-12Rβ2* gene in WKAH rats. However, functional studies are required to understand whether this polymorphism is biologically significant.

In WKAH rats, HTLV-1 infection did not up-regulate *IL-12Rβ2* gene expression in the cerebrum (Figure 7). This observation was initially puzzling because the cerebrum of WKAH rats was able to produce IFN-γ in response to HTLV-1 infection (Figure 1A). A solution to this apparent paradox came from the fact that production of IFN-γ is regulated not only by IL-12 but also by IL-23 and IL-27.[41] We observed that HTLV-1 infection increased the amount of mRNA for IL-23, IL-27, and their receptors in the cerebrum but not in the spinal cord of WKAH rats (Figure 8). Thus, alternative pathways of IFN-γ induction are active in the cerebrum of WKAH rats. We suggest that induction of IFN-γ via IL-12-independent pathways explains at least in part why the cerebrum is never affected in HAM rat disease.

In conclusion, this study is the first to indicate that neuronal IFN-γ protects the CNS from tissue damage caused by HTLV-1 infection. Although *IL-12Rβ2* is a prime candidate for the gene that controls susceptibility to HAM rat disease, genes involved in the regulation of *IL-12Rβ2* are also potential candidates. We envision that IL-12/IL-12 receptor-mediated, neuronal IFN-γ responses are also critically involved in the pathogenesis of human HAM/TSP. Hence, the dissection of the molecular mechanisms leading to the development of HAM rat disease should help us understand the factors that govern susceptibility to human HAM/TSP.

Acknowledgments

We thank the entire staff of the Institute of Animal Experimentation, Hokkaido University Graduate School of Medicine for their skillful maintenance of rats.

References

1. Poiesz BJ, Ruscetti FW, Gazdar AF, Bunn PA, Minna JD, Gallo RC: Detection and isolation of type C retrovirus particles from fresh and cultured lymphocytes of a patient with cutaneous T-cell lymphoma. Proc Natl Acad Sci USA 1980, 77:7415–7419
2. Yoshida M, Miyoshi I, Hinuma Y: Isolation and characterization of

retrovirus from cell lines of human adult T-cell leukemia and its implication in the disease. Proc Natl Acad Sci USA 1982, 79:2031–2035
3. Gessain A, Barin F, Vernant JC, Gout O, Maurs L, Calender A, de Thé G: Antibodies to human T-lymphotropic virus type-I in patients with tropical spastic paraparesis. Lancet 1985, 2:407–410
4. Osame M, Usuku K, Izumo S, Ijichi N, Amitani H, Igata A, Matsumoto M, Tara M: HTLV-I associated myelopathy, a new clinical entity. Lancet 1986, 1:1031–1032
5. Mochizuki M, Watanabe T, Yamaguchi K, Takatsuki K, Yoshimura K, Shirao M, Nakashima S, Mori S, Araki S, Miyata N: HTLV-I uveitis: a distinct clinical entity caused by HTLV-I. Jpn J Cancer Res 1992, 83:236–239
6. Nishioka K, Maruyama I, Sato K, Kitajima I, Nakajima Y, Osame M: Chronic inflammatory arthropathy associated with HTLV-I. Lancet 1989, 1:441
7. Sugimoto M, Nakashima H, Watanabe S, Uyama E, Tanaka F, Ando M, Araki S, Kawasaki S: T-lymphocyte alveolitis in HTLV-I-associated myelopathy. Lancet 1987, 2:1220
8. Vernant JC, Buisson G, Magdeleine J, De Thore J, Jouannelle A, Neisson-Vernant C, Monplaisir N: T-lymphocyte alveolitis, tropical spastic paresis, and Sjögren syndrome. Lancet 1988, 1:177
9. Morgan OS, Rodgers-Johnson P, Mora C, Char G: HTLV-1 and polymyositis in Jamaica. Lancet 1989, 2:1184–1187
10. LaGrenade L, Hanchard B, Fletcher V, Cranston B, Blattner W: Infective dermatitis of Jamaican children: a marker for HTLV-I infection. Lancet 1990, 336:1345–1347
11. Hollsberg P, Hafler DA: Seminars in medicine of the Beth Israel Hospital, Boston. Pathogenesis of diseases induced by human lymphotropic virus type I infection. N Engl J Med 1993, 328:1173–1182
12. Ishiguro N, Abe M, Seto K, Sakurai H, Ikeda H, Wakisaka A, Togashi T, Tateno M, Yoshiki T: A rat model of human T lymphocyte virus type I (HTLV-I) infection. 1. Humoral antibody response, provirus integration, and HTLV-I-associated myelopathy/tropical spastic paraparesis-like myelopathy in seronegative HTLV-I carrier rats. J Exp Med 1992, 176:981–989
13. Seto K, Abe M, Ohya O, Itakura O, Ishiguro N, Ikeda H, Wakisaka A, Yoshiki T: A rat model of HTLV-I infection: development of chronic progressive myeloneuropathy in seropositive WKAH rats and related apoptosis. Acta Neuropathol (Berl) 1995, 89:483–490
14. Ohya O, Ikeda H, Tomaru U, Yamashita I, Kasai T, Morita K, Wakisaka A, Yoshiki T: Human T-lymphocyte virus type I (HTLV-I)-induced myeloneuropathy in rats: oligodendrocytes undergo apoptosis in the presence of HTLV-I. APMIS 2000, 108:459–466
15. Jacobson S: Immunopathogenesis of human T cell lymphotropic virus type I-associated neurologic disease. J Infect Dis 2002, 186(Suppl 2):S187–S192
16. Kasai T, Ikeda H, Tomaru U, Yamashita I, Ohya O, Morita K, Wakisaka A, Matsuoka E, Moritoyo T, Hashimoto K, Higuchi I, Izumo S, Osame M, Yoshiki T: A rat model of human T lymphocyte virus type I (HTLV-I) infection: in situ detection of HTLV-I provirus DNA in microglia/macrophages in affected spinal cords of rats with HTLV-I-induced chronic progressive myeloneuropathy. Acta Neuropathol (Berl) 1999, 97:107–112
17. Tomaru U, Ikeda H, Ohya O, Abe M, Kasai T, Yamasita I, Morita K, Wakisaka A, Yoshiki T: Human T lymphocyte virus type I-induced myeloneuropathy in rats: implication of local activation of the pX and tumor necrosis factor-alpha genes in pathogenesis. J Infect Dis 1996, 174:318–323
18. Jiang X, Ikeda H, Tomaru U, Morita K, Tanaka Y, Yoshiki T: A rat model for human T lymphocyte virus type I-associated myeloneuropathy. Down-regulation of bcl-2 expression and increase in sensitivity to TNF-alpha of the spinal oligodendrocytes. J Neuroimmunol 2000, 106:105–113
19. Panitch HS, Hirsch RL, Haley AS, Johnson KP: Exacerbations of multiple sclerosis in patients treated with gamma interferon. Lancet 1987, 1:893–895
20. Renno T, Taupin V, Bourbonniere L, Verge G, Tran E, De Simone R, Krakowski M, Rodriguez M, Peterson A, Owens T: Interferon-gamma in progression to chronic demyelination and neurological deficit following acute EAE. Mol Cell Neurosci 1998, 12:376–389
21. Krakowski M, Owens T: Interferon-gamma confers resistance to experimental allergic encephalomyelitis. Eur J Immunol 1996, 26:1641–1646
22. Gao X, Gillig TA, Ye P, D'Ercole AJ, Matsushima GK, Popko B: Interferon-gamma protects against cuprizone-induced demyelination. Mol Cell Neurosci 2000, 16:338–349
23. Finke D, Brinckmann UG, ter Meulen V, Liebert UG: Gamma interferon is a major mediator of antiviral defense in experimental measles virus-induced encephalitis. J Virol 1995, 69:5469–5474
24. Patterson CE, Lawrence DM, Echols LA, Rall GF: Immune-mediated protection from measles virus-induced central nervous system disease is noncytolytic and gamma interferon dependent. J Virol 2002, 76:4497–4506
25. Geiger KD, Nash TC, Sawyer S, Krahl T, Patstone G, Reed JC, Krajewski S, Dalton D, Buchmeier MJ, Sarvetnick N: Interferon-gamma protects against herpes simplex virus type 1-mediated neuronal death. Virology 1997, 238:189–197
26. Miyoshi I, Kubonishi I, Yoshimoto S, Akagi T, Ohtsuki Y, Shiraishi Y, Nagata K, Hinuma Y: Type C virus particles in a cord T-cell line derived by co-cultivating normal human cord leukocytes and human leukaemic T cells. Nature 1981, 294:770–771
27. Bloch G, Toma DP, Robinson GE: Behavioral rhythmicity, age, division of labor and period expression in the honey bee brain. J Biol Rhythms 2001, 16:444–456
28. Pelidou SH, Zou LP, Deretzi G, Nennesmo I, Wei L, Mix E, Van Der Meide PH, Zhu J: Intranasal administration of recombinant mouse interleukin-12 increases inflammation and demyelination in chronic experimental autoimmune neuritis in Lewis rats. Scand J Immunol 2000, 51:29–35
29. Tomaru U, Ikeda H, Jiang X, Ohya O, Yoshiki T: Provirus expansion and deregulation of apoptosis-related genes in the spinal cord of a rat model for human T-lymphocyte virus type I-associated myeloneuropathy. J Neurovirol 2003, 9:530–538
30. Kroger A, Koster M, Schroeder K, Hauser H, Mueller PP: Activities of IRF-1. J Interferon Cytokine Res 2002, 22:5–14
31. D'Onofrio C, Franzese O, Puglianiello A, Peci E, Lanzilli G, Bonmassar E: Antiviral activity of individual versus combined treatments with interferon alpha, beta and gamma on early infection with HTLV-I in vitro. Int J Immunopharmacol 1992, 14:1069–1079
32. Neumann H, Schmidt H, Wilharm E, Behrens L, Wekerle H: Interferon gamma gene expression in sensory neurons: evidence for autocrine gene regulation. J Exp Med 1997, 186:2023–2031
33. Olsson T, Kelic S, Edlund C, Bakhiet M, Hojeberg B, van der Meide PH, Ljungdahl A, Kristensson K: Neuronal interferon-gamma immunoreactive molecule: bioactivities and purification. Eur J Immunol 1994, 24:308–314
34. Schmidt B, Stoll G, Toyka KV, Hartung HP: Rat astrocytes express interferon-gamma immunoreactivity in normal optic nerve and after nerve transection. Brain Res 1990, 515:347–350
35. Barish ME, Mansdorf NB, Raissdana SS: Gamma-interferon promotes differentiation of cultured cortical and hippocampal neurons. Dev Biol 1991, 144:412–423
36. Vikman K, Robertson B, Grant G, Liljeborg A, Kristensson K: Interferon-gamma receptors are expressed at synapses in the rat superficial dorsal horn and lateral spinal nucleus. J Neurocytol 1998, 27:749–759
37. Frucht DM, Fukao T, Bogdan C, Schindler H, O'Shea JJ, Koyasu S: IFN-gamma production by antigen-presenting cells: mechanisms emerge. Trends Immunol 2001, 22:556–560
38. Watford WT, Moriguchi M, Morinobu A, O'Shea JJ: The biology of IL-12: coordinating innate and adaptive immune responses. Cytokine Growth Factor Rev 2003, 14:361–368
39. van Rietschoten JG, Smits HH, van de Wetering D, Westland R, Verweij CL, den Hartog MT, Wierenga EA: Silencer activity of NFATc2 in the interleukin-12 receptor beta 2 proximal promoter in human T helper cells. J Biol Chem 2001, 276:34509–34516
40. van Rietschoten JG, Westland R, van den Bogaard R, Nieste-Otter MA, van Veen A, Jonkers RE, van der Pouw Kraan TC, den Hartog MT, Wierenga EA: A novel polymorphic GATA site in the human IL-12Rbeta2 promoter region affects transcriptional activity. Tissue Antigens 2004, 63:538–546
41. Rosenzweig SD, Holland SM: Defects in the interferon-gamma and interleukin-12 pathways. Immunol Rev 2005, 203:38–47
42. Watford WT, Hissong BD, Bream JH, Kanno Y, Muul L, O'Shea JJ: Signaling by IL-12 and IL-23 and the immunoregulatory roles of STAT4. Immunol Rev 2004, 202:139–156
43. Xiao BG, Link H: Immune regulation within the central nervous system. J Neurol Sci 1998, 157:1–12

44. Eneroth A, Andersson T, Olsson T, Orvell C, Norrby E, Kristensson K: Interferon-gamma-like immunoreactivity in sensory neurons may influence the replication of Sendai and mumps viruses. J Neurosci Res 1992, 31:487–493
45. Kohanawa M, Nakane A, Asano M, Minagawa T: Theiler's virus is eliminated by a gamma-interferon-independent mechanism in the brain. J Neuroimmunol 1994, 52:79–86
46. Kiefer R, Haas CA, Kreutzberg GW: Gamma interferon-like immunoreactive material in rat neurons: evidence against a close relationship to gamma interferon. Neuroscience 1991, 45:551–560
47. Lau LT, Yu AC: Astrocytes produce and release interleukin-1, interleukin-6, tumor necrosis factor alpha and interferon-gamma following traumatic and metabolic injury. J Neurotrauma 2001, 18:351–359
48. Xiao BG, Link H: IFN-gamma production of adult rat astrocytes triggered by TNF-alpha. Neuroreport 1998, 9:1487–1490
49. Li J, Gran B, Zhang GX, Ventura ES, Siglienti I, Rostami A, Kamoun M: Differential expression and regulation of IL-23 and IL-12 subunits and receptors in adult mouse microglia. J Neurol Sci 2003, 215:95–103

MHC Class I-Like MILL Molecules Are β_2-Microglobulin-Associated, GPI-Anchored Glycoproteins That Do Not Require TAP for Cell Surface Expression[1]

Mizuho Kajikawa,*† Tomohisa Baba,‡ Utano Tomaru,‡ Yutaka Watanabe,* Satoru Koganei,§ Sachiyo Tsuji-Kawahara,¶ Naoki Matsumoto,§ Kazuo Yamamoto,§ Masaaki Miyazawa,¶ Katsumi Maenaka,† Akihiro Ishizu,‡‖ and Masanori Kasahara[2]*‡

MILL (MHC class I-like located near the leukocyte receptor complex) is a family of MHC class I-like molecules encoded outside the MHC, which displays the highest sequence similarity to human MICA/B molecules among known class I molecules. In the present study, we show that the two members of the mouse MILL family, MILL1 and MILL2, are GPI-anchored glycoproteins associated with β_2-microglobulin (β_2m) and that cell surface expression of MILL1 or MILL2 does not require functional TAP molecules. MILL1 and MILL2 molecules expressed in bacteria could be refolded in the presence of β_2m, without adding any peptides. Hence, neither MILL1 nor MILL2 is likely to be involved in the presentation of peptides. Immunohistochemical analysis revealed that MILL1 is expressed in a subpopulation of thymic medullary epithelial cells and a restricted region of inner root sheaths in hair follicles. The present study provides additional evidence that MILL is a class I family distinct from MICA/B. *The Journal of Immunology,* **2006, 177: 3108–3115.**

Classical MHC class I molecules, also known as class Ia, are heterodimeric glycoproteins made up of a transmembrane-type H chain and β_2-microglobulin (β_2m).[3] They bind small peptides primarily derived from cytosolic proteins in a groove comprised of the α1 and α2 domains and present them to $CD8^+$ T cells, thereby enabling the immune system to destroy abnormal cells that synthesize viral or other foreign proteins (1). Class Ia molecules are almost ubiquitously expressed and their H chains exhibit an extraordinary level of polymorphism (2).

By contrast, class I molecules, collectively called nonclassical class I or class Ib, are usually oligomorphic or monomorphic, and do not necessarily bind peptides (3–5). Many class Ib molecules have a more restricted tissue distribution than class Ia molecules. Although the majority of class Ib molecules form complexes with β_2m, MICA/B (MHC class I-related chains A and B) (6), zinc-α2-glycoprotein (7), the endothelial protein C receptor (8), and the RAE-1 (retinoic acid early inducible-1) family of class Ib molecules (9) are not associated with β_2m. Furthermore, a significant proportion of class Ib genes (the genes coding for the H chains of class Ib molecules) are located outside the MHC region (5). Accumulated evidence indicates that class Ib molecules have diverse functions ranging from specialized Ag presentation (10–12) to the activation of NK cells (13, 14), transport of IgG (15), pheromone detection (16, 17), and lipid mobilization and catabolism (18).

Recently, we identified a new family of class Ib genes designated *Mill* (MHC class I-like located near the leukocyte receptor complex) in mice (19) and rats (20). The two members of the *Mill* family, *Mill1* and *Mill2*, are located close to the leukocyte receptor complex, thus outside the MHC. *Mill1* and *Mill2* show only limited levels of polymorphism and are transcribed at low levels in most adult tissues. RT-PCR analysis showed that *Mill1* is transcribed in selected tissues such as neonatal thymus and skin whereas *Mill2* is transcribed more ubiquitously at low levels. Predicted MILL1 and MILL2 molecules are glycoproteins with three extracellular domains (α1 to α3), but their α1 and α2 domains lack many of the residues essential for the docking of peptides, suggesting that MILL molecules do not bind peptides. Phylogenetically, MILL1 and MILL2 are most closely related to MICA/B among known class I molecules. Because rodents lack the MICA/B family and conversely, humans do not have the MILL family, we suggested previously that MILL might be a functional substitute for MICA/B (19).

In the present study, we show that MILL1 and MILL2 are GPI-anchored glycoproteins associated with β_2m. Consistent with the absence of critical residues required for the docking of peptides (19), cell surface expression of MILL1 and MILL2 did not require TAP molecules. Immunohistochemical analysis revealed that MILL1 is expressed in a subpopulation of thymic medullary epithelial cells and a restricted region of inner root sheaths in hair follicles. The ability to form complexes with β_2m, anchorage to the membrane by GPI, and unique expression patterns all provide further evidence that MILL is a class I family distinct from MICA/B.

*Department of Biosystems Science, School of Advanced Sciences, Graduate University for Advanced Studies (Sokendai), Hayama, Japan; †Division of Structural Biology, Medical Institute of Bioregulation, Kyushu University, Fukuoka, Japan; ‡Department of Pathology, Hokkaido University Graduate School of Medicine, Sapporo, Japan; §Department of Integrated Biosciences, Graduate School of Frontier Sciences, University of Tokyo, Chiba, Japan; ¶Department of Immunology, Kinki University School of Medicine, Osaka, Japan; and ‖Department of Medical Technology, Hokkaido University School of Medicine, Sapporo, Japan

Received for publication July 26, 2005. Accepted for publication June 16, 2006.

The costs of publication of this article were defrayed in part by the payment of page charges. This article must therefore be hereby marked *advertisement* in accordance with 18 U.S.C. Section 1734 solely to indicate this fact.

[1] This work was supported by grants-in-aid for Scientific Research from the Ministry of Education, Culture, Sports, Science and Technology of Japan, Uehara Memorial Foundation, the Naito Foundation, and the Takeda Science Foundation.

[2] Address correspondence and reprint requests to Dr. Masanori Kasahara, Department of Pathology, Hokkaido University Graduate School of Medicine, North-15, West-7, Sapporo 060-8638, Japan. E-mail address: mkasaha@med.hokudai.ac.jp

[3] Abbreviations used in this paper: β_2m, β_2-microglobulin; MILL, MHC class I-like located near the leukocyte receptor complex; PI-PLC, phosphatidylinositol-specific phospholipase C; PNGase F, peptide:*N*-glycosidase F.

0022-1767/06/$02.00

Materials and Methods

Cell lines and Abs

The mouse T lymphoma cell line RMA ($H2^b$-positive) and its TAP2-deficient mutant RMA-S ($H2^b$-negative) (21) were obtained from Dr. Kärre (Karolinska Institute, Stockholm, Sweden). Cells were maintained in RPMI 1640 medium (Invitrogen) supplemented with 10% (v/v) heat-inactivated FBS at 37°C and 5% CO_2.

Anti-FLAG mAb M2 (F3165) was purchased from Sigma-Aldrich. Goat polyclonal Ab to mouse β_2m (sc-8361) was purchased from Santa Cruz Biotechnology. Anti-human pan-cytokeratin mAb AE1/AE3 (M1590) and anti-human hair shaft cytokeratin mAb AE13 (ab16113) were purchased from DakoCytomation and Abcam, respectively. Mouse anti-H2-K^b mAb (clone AF6–88.5) and anti-CD45 mAb (clone 30-F11) were from BD Pharmingen. The Abs used as secondary reagents were as follows: FITC-labeled goat anti-mouse IgG, $F(ab')_2$ fragment (IM0819; Beckman Coulter), FITC-labeled swine anti-rabbit Ig, $F(ab')_2$ fragment (F0054; DakoCytomation), HRP-conjugated sheep anti-mouse IgG (NA931; Amersham Biosciences), HRP-conjugated donkey anti-rabbit IgG (NA934; Amersham Biosciences), HRP-conjugated donkey anti-goat IgG (sc-2056; Santa Cruz Biotechnology), Alexa Fluor 594-conjugated goat anti-rabbit IgG (A11072; Molecular Probes), and Alexa Fluor 488-conjugated goat anti-mouse IgG (A11001; Molecular Probes). Isotype-matched mouse IgG1 Ab (PP100) and pooled normal rabbit serum (CL1000) were purchased from Chemicon International Inc. and Cedarlane Laboratory Ltd., respectively.

Production of polyclonal Ab against mouse MILL molecules

The α1-α3 domains of MILL1 and MILL2 with 6 × His tags at their N termini were expressed in *Escherichia coli* strain M15 using the pQE30 expression vector following the instructions of the manufacturer (Qiagen). Briefly, the DNA fragments encoding the α1-α3 domains of mouse MILL molecules were amplified by PCR using the BALB/c-derived *Mill* plasmid cDNA (19) as templates. The primer sequences were 5′-TTGCGAGCTC CACACTCTGCGCTATGACCT-3′ (with a *Sac*I site at its 5′-end) and 5′-CCCAAGCTTATATTGTGGTTGCCGTGCTT-3′ (with a *Hin*dIII site at its 5′-end) for MILL1 and 5′-GTGGATCCACCCACACTCTGCGC TATAA-3′ (with a *Bam*HI site at its 5′-end) and 5′-CCCAAGCTTCATC CTGACTGTCCTCAGCA-3′ (with a *Hin*dIII site at its 5′-end) for MILL2. PCR products digested with *SacI*/*Hin*dIII for MILL1 and *Bam*HI/*Hin*dIII for MILL2 were ligated into *SacI*/*Hin*dIII- and *Bam*HI/*Hin*dIII-digested pQE30, respectively. After transformation into M15, recombinant proteins were induced by adding isopropyl-1-thio-β-D-galactopyranoside to a final concentration of 1 mM. *E. coli* cells were harvested and lysed in buffer B (100 mM NaH_2PO_4, 10 mM Tris-HCl, 6 M guanidine hydrochloride, pH 8.0), and lysates were centrifuged at 10,000 × *g* for 20 min at room temperature. Ni-NTA acid resins were added to supernatants and mixed gently by shaking. Resin-lysate mixtures were loaded into an empty column and washed twice with buffer C (100 mM NaH_2PO_4, 10 mM Tris-HCl, 6 M guanidine hydrochloride, pH 5.9). Recombinant proteins were eluted by buffer D (100 mM NaH_2PO_4, 10 mM Tris-HCl, 6 M guanidine hydrochloride, pH 4.5), separated by preparative SDS-PAGE, eluted and concentrated. Purified recombinant proteins (200 μg per rabbit) were mixed with CFA and injected into rabbits. After 2, 4, and 6 wk, the animals were boosted with the same amount of recombinant proteins mixed with IFA. Whole bloods were collected and antisera prepared 1 wk after the last boost.

Construction of mammalian expression plasmids

Mouse MILL molecules have an insertion of amino acids between the leader peptide and the α1 domain (19). The coding regions of mouse MILL1 and MILL2 excluding this inserted sequence and the leader peptide were obtained by PCR using the *Mill* plasmid cDNA (19) as templates. The primer sequences were 5′-CCAAGCTTGAACCCCACACTCTGCGC TA-3′ (with a *Hin*dIII site at its 5′-end) and 5′-GTGGATCCCTACCAA CACTGTAGAAAAGAGC-3′ (with a *Bam*HI site at its 5′-end) for MILL1 and 5′-CCAAGCTTACCCACACTCTGCGCTATAA-3′ (with a *Hin*dIII site at its 5′-end) and 5′-GTGGATCCTCAGTTGGCTCTGGCCAGTG-3′ (with a *Bam*HI site at its 5′-end) for MILL2. After digestion with *Hin*dIII/*Bam*HI, the PCR products were ligated to the *Hin*dIII/*Bam*HI-digested pFLAG-CMV-3 expression vector carrying a preprotrypsin leader sequence (Sigma-Aldrich). These constructs, designated MILL1-pFLAG-CMV-3 and MILL2-pFLAG-CMV-3, respectively, enabled the expression of MILL molecules with an N-terminal FLAG tag. In all cases, the integrity of expression constructs was verified by sequencing. DNA for transfection was isolated with the plasmid purification kit purchased from Qiagen.

Establishment of stable transfectants

To establish stable cell lines expressing MILL molecules, RMA and RMA-S cells were transfected with linearized MILL1-pFLAG-CMV-3 or MILL2-pFLAG-CMV-3 plasmids by electroporation at 250 V, 950 μF with Gene Pulser II according to the instructions of the manufacturer (Bio-Rad). Neomycin-resistant cells were selected by treatment with G418 (600 and 800 μg/ml for RMA and RMA-S, respectively) and clones exhibiting high levels of MILL expression were expanded; expression of MILL proteins was monitored by flow cytometry and immunoblotting with anti-FLAG and anti-MILL Abs.

Flow cytometric analysis

For cell surface staining, single cell suspensions (1 × 10^6 cells) were washed with ice-cold PBS (pH 7.4) and incubated in 100 μl of PBS (pH 7.4) containing 0.1% NaN_3 with 1 μg of mAb or isotype controls for 30 min on ice. After washing with ice-cold PBS (pH 7.4), cells were incubated in 100 μl of PBS (pH 7.4) containing 0.1% NaN_3 with the FITC-conjugated F(ab′) fragment of goat anti-mouse IgG or $F(ab')_2$ fragment of swine anti-rabbit Ig (1:200 dilution). Subsequently, cells were washed with ice-cold PBS (pH 7.4) and analyzed by EPICS ALTRA (Beckman Coulter). Data were analyzed with EXPO32 software (Beckman Coulter).

Immunoprecipitation and glycosidase digestion

For purification of FLAG-tagged MILL proteins, RMA-MILL1 and RMA-MILL2 stable transfectants (1 × 10^8 cells) were solubilized by 1 ml of ice-cold lysis buffer (50 mM Tris-HCl, 1 mM EDTA, 150 mM NaCl, 1% Triton X-100, 0.2 mM 4-(2-aminoethyl)-benzenesulfonyl fluoride, 20 μM leupeptin, 1 μM pepstatin, pH 7.5). After incubation for 30 min at 4°C, cell lysates were centrifuged at 13,000 × *g* for 10 min at 4°C to remove cell nuclei and insoluble proteins. Cleared lysates were incubated with protein G-Sepharose beads (Amersham Biosciences) at 4°C for 1 h. Supernatants were incubated with anti-FLAG mAb-coupled protein G-Sepharose beads at 4°C for 1 h. After washing 4 times with lysis buffer, immunoprecipitated proteins were eluted by 0.1 M glycine-HCl (pH 3.0), and immediately neutralized by adding 0.1 M Tris-HCl (pH 9.0). Eluted proteins were denatured and treated with 500 U/μl peptide:*N*-glycosidase F (PNGase F; New England Biolabs) at 37°C for 18 h.

Immunoblotting

To detect MILL proteins and β_2m, samples were incubated in 1 × SDS sample buffer at 95°C for 10 min. Denatured proteins were separated on 12% SDS-PAGE and transferred to Hybond-P polyvinylidene difluoride membranes (Amersham Biosciences) using a semidry blotter (Bio-Rad) at 15 V for 45 min. The blotted membranes were incubated with 5% skim milk or 3% BSA in PBS (pH 7.4) containing 0.1% Tween 20 (PBST) at room temperature for 60 min and then incubated with 1/500 diluted antisera or 1 μg/ml of Ab in PBST at room temperature for 60 min. After washing twice with PBST, the membranes were incubated with 1/25,000 diluted HRP-conjugated anti-mouse, rabbit or goat IgG Abs. After washing three times with PBST, positive bands were visualized using the ECL-Plus (Amersham Biosciences) or the Super Signal West Dura detection system (Pierce).

Phosphatidylinositol-specific phospholipase C (PI-PLC) treatment

RMA-MILL and RMA-S-MILL cells were washed with PBS (pH 7.4) and treated with 1 U/ml PI-PLC (Sigma-Aldrich) in PBS (pH 7.4) at 37°C for 1 h. Subsequently, cells were washed with ice-cold PBS (pH 7.4) and used for flow cytometric analysis.

Coimmunoprecipitation of cell surface MILL molecules

Cell surface MILL proteins expressed on the RMA-MILL stable transfectants were purified by PI-PLC treatment and immunoprecipitation with anti-FLAG Ab-coupled protein G-Sepharose beads. Immunoprecipitates were subjected to immunoblotting using anti-FLAG and anti-mouse β_2m Ab.

Refolding of bacterially expressed MILL ectodomains

cDNA encoding the ectodomains of MILL1 and MILL2 were amplified by PCR using the *Mill* plasmid cDNA (19) as templates. Primers used were 5′-CATTAATGGACAACCAAAGACTGGTG-3′ (sense) and 5′-TCC CCCGGGGGCAGCAGGTTCATTGATA-3′ (antisense) for MILL1, and 5′-CCATATGTCCAGCATCCAAGGAACC-3′ (sense) and 5′-AAAAG TACTGACAGCTGTCTGCATGATG-3′ (antisense) for MILL2. These

primers contained *AseI*, *SmaI*, *NdeI*, or *ScaI* restriction enzyme sites indicated by underlines. The PCR-generated cDNA fragments of MILL1 and MILL2 were cloned into the bacterial expression vector pET3cN-bio, which was designed to express a recombinant protein with an N-terminal enzymatic biotinylation signal (22), to construct MILL1-pET3cNbio and MILL2-pET3cNbio, respectively. Rosetta (DE3) strain of *E. coli* (Novagen, Merck) was transformed with MILL1-pET3cNbio or MILL2-pET3cNbio. Expression of soluble MILL1 or MILL2 was induced with 1 mM isopropyl-1-thio-β-D-galactopyranoside, and MILL proteins were refolded from the purified inclusion bodies by dilution as described previously (22). To examine effects of β_2m on refolding, C57BL/6-derived β_2m (β_2m^b), similarly expressed in *E. coli*, was included in the refolding mixture at the molar ratio of 1:2 (MILL/β_2m). Refolded soluble MILL1 and MILL2 proteins were purified by anion-exchange column chromatography and gel-filtration chromatography. In anion-exchange chromatography on a UNO Q-6 column using 20 mM Tris-HCl buffer (pH 8.5) as a mobile phase, soluble MILL1 or MILL2 refolded in the presence of β_2m was eluted in the approximately 250 mM Cl^- fraction by a 0–500 mM NaCl gradient. The gel-filtration column chromatography was performed on a Superdex 75 10/30 column (Amersham Biosciences) equilibrated with 25 mM Tris-HCl buffer (pH 8.0) containing 150 mM NaCl at the flow rate of 0.5 ml/min. The column was calibrated with gel-filtration standards from Bio-Rad.

Immunohistochemistry

For immunostaining, frozen sections prepared from 3-day-old, 10-day-old, and 6-wk-old male BALB/c mice were fixed using cold acetone for 5 min, washed with PBS, stained by the standard method (23), and then mounted in fluorescent mounting medium (DakoCytomation). Immunofluorescence was detected using a fluorescence microscope (ECLIPSE E600; Nikon). To evaluate the specificity of staining, the antiserum against MILL1 was diluted 1/40 with PBS to a final volume of 1 ml and absorbed with 5×10^7 RMA-MILL1 or RMA cells at 4°C overnight. The preabsorbed antiserum was diluted 1/80 with PBS and used for immunostaining. All experiments using animals have been reviewed and approved by the institutional review committee of Hokkaido University Graduate School of Medicine.

Isolation of thymic stromal cells

Thymi were dissected from 4-wk-old C57BL/6 and β_2m-deficient mice. Breeding pairs of the β_2m-deficient strain, B6.129P2-*B2m*^{tm1Unc}/J (stock no. 002087), were purchased from The Jackson Laboratory, and their progenies were produced at Kinki University School of Medicine. Thymic stromal cells were enriched as described (24). Briefly, thymic fragments were digested in RPMI 1640 medium containing collagenase D and DNase I (both obtained from Roche) at 37°C for 15 min. After repeating this procedure 3 times, cells were pooled and stained with mAb for CD45. CD45-negative fractions containing stromal cells including thymic epithelial cells were subjected to flow cytometric analysis.

Results

Establishment of stable cell lines expressing N-terminally FLAG-tagged MILL molecules and generation of rabbit antisera specific for MILL molecules

To facilitate biochemical analysis, we transfected FLAG-tagged expression plasmids into the mouse T lymphoma cell line RMA and established stable cell lines, RMA-MILL1 and RMA-MILL2, expressing N-terminally FLAG-tagged MILL1 and MILL2 molecules, respectively (Fig. 1*A*). Cell surface expression of MILL1 and MILL2 was confirmed by flow cytometry using the anti-FLAG Ab as well as the rabbit antisera generated against bacterially expressed MILL1 and MILL2 molecules. The specificity of our rabbit antisera was further confirmed by Western blot analysis of whole cell lysates (Fig. 1*B*). The anti-FLAG Ab detected two major bands of 48 and 41 kDa in RMA-MILL1 cells. The band of 41 kDa was nonspecific because it was detected in untransfected RMA cells. A major band of 48 kDa and a minor band of 44 kDa were detected by the anti-MILL1, but not anti-MILL2, antiserum (Fig. 1*B*). In RMA-MILL2 lysates, the anti-FLAG Ab detected bands of 43 and 41 kDa (Fig. 1*B*, *top*), which were also detected with the anti-MILL2, but not anti-MILL1, antiserum (Fig. 1*B*, *bottom*). Thus, the band of 41 kDa detected by the anti-FLAG Ab in RMA-MILL2 cells presumably represents doublets containing both specific and nonspecific signals. We also expressed MILL1 and MILL2 molecules on RMA cells using their endogenous signal peptides and performed cytometric analysis using the MILL-specific rabbit antisera. We obtained staining patterns similar to those shown in Fig. 1*A* (data not shown).

Deduced MILL1 and MILL2 molecules have three potential *N*-linked glycosylation sites, respectively (19). To examine glycosylation status, we isolated MILL molecules from the stable transfectants by immunoprecipitation with the anti-FLAG Ab, removed

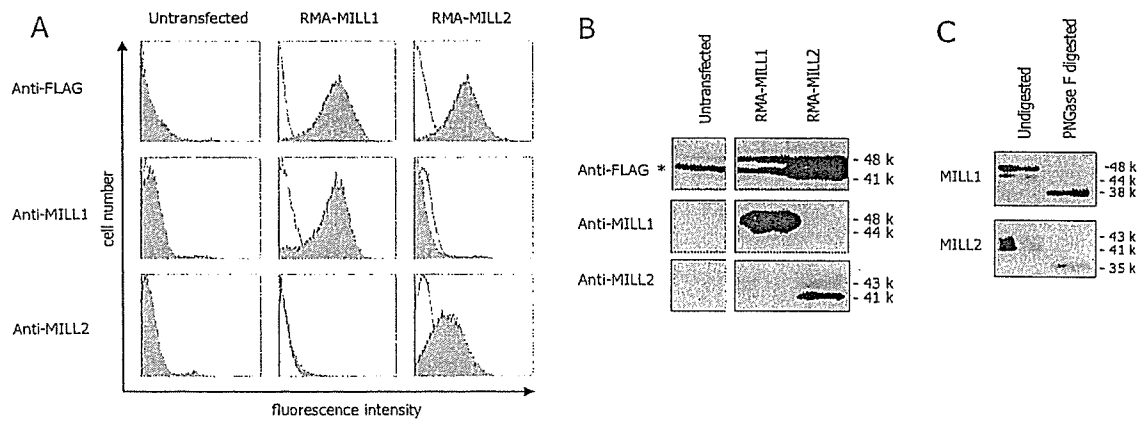

FIGURE 1. MILL1 and MILL2 are cell surface glycoproteins with *N*-linked sugars. *A*, Untransfected RMA cells and the transfected cell lines, RMA-MILL1 and RMA-MILL2, which stably express MILL1 and MILL2, respectively, were incubated with anti-FLAG mAb and FITC-conjugated goat anti-mouse IgG, anti-MILL1 antiserum (1/500 dilution) and FITC-labeled swine anti-rabbit Ig, or anti-MILL2 antiserum (1/500 dilution) and FITC-labeled swine anti-rabbit Ig (from the top to the bottom, shaded histograms). Negative control staining (open histograms) was obtained using an isotype-matched control Ab (top three panels) or normal rabbit serum (all other panels). Stained cells were analyzed by flow cytometry. *B*, Whole cell lysates of RMA-MILL1 and RMA-MILL2 were separated on 12% SDS-PAGE and subjected to immunoblotting using anti-FLAG mAb (top), anti-MILL1 antiserum (middle), or anti-MILL2 antiserum (bottom). Signals were detected by HRP-conjugated secondary Ab and ECL-Plus reagents. Nonspecific bands are indicated by asterisks. *C*, MILL1 and MILL2 proteins were immunoprecipitated with anti-FLAG mAb-coupled protein G-Sepharose beads from RMA-MILL1 and RMA-MILL2 cell lysates, respectively. After digestion with PNGase F at 37°C for 18 h, samples were separated on 12% SDS-PAGE and subjected to immunoblotting. MILL1 was detected by the rabbit anti-MILL1 antiserum and MILL2 by the rabbit anti-MILL2 antiserum. Signals were detected by HRP-conjugated secondary Ab and ECL-Plus reagents.

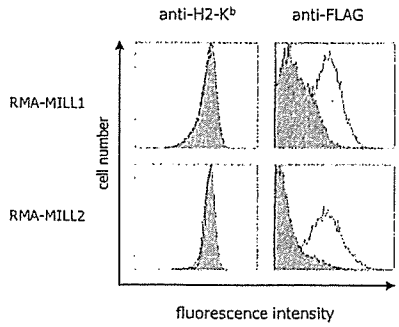

FIGURE 2. MILL1 and MILL2 are GPI-anchored proteins. RMA-MILL1 and RMA-MILL2 cells (top and bottom, respectively) were incubated with 1 U/ml PI-PLC (shaded histograms) or PBS (open histograms). Subsequently, cells were stained with anti-H2-K^b (left) or anti-FLAG (right) mAb. An FITC-conjugated F(ab')$_2$ fragment of goat anti-mouse IgG was used as a secondary Ab. Stained cells were analyzed by flow cytometry.

N-linked glycans with PNGase F and performed immunoblot analysis with the MILL-specific antisera (Fig. 1*C*). We obtained two bands of 44 and 48 kDa for non-treated MILL1, and a single band of 38 kDa for PNGase F-treated MILL1 (Fig. 1*C*, *top*). Similarly, we obtained two bands of 41 and 43 kDa for non-treated MILL2, and a single band of 35 kDa for PNGase F-treated MILL2 (Fig. 1*C*, *bottom*). The expression constructs used for stable transfection predicted M_r of 39280.83 and 35013.86 for the protein moieties of N-terminally flagged MILL1 and MILL2 molecules, respectively. Thus, the sizes of deglycosylated products agreed well with theoretical expectations. These results indicate that MILL1 and MILL2 are cell surface glycoproteins with *N*-linked sugars.

MILL1 and MILL2 are GPI-anchored proteins

We initially assumed that MILL1 and MILL2 were transmembrane proteins (19, 20). However, different prediction algorithms yielded inconsistent results concerning the presence or absence of transmembrane regions. Subsequent sequence analysis using the software 'big-PI Predictor' (25) suggested that MILL1 and MILL2 were likely GPI-anchored proteins. To examine this possibility, RMA-MILL1 and RMA-MILL2 cells were treated with PI-PLC, stained with the anti-FLAG Ab and examined by flow cytometry. In both RMA-MILL1 and RMA-MILL2 cells, cell surface staining was reduced markedly by PI-PLC treatment (Fig. 2, *right panel*). By contrast, cell surface staining with the H2-K^b Ab was not affected by similar treatment (Fig. 2, *left panel*), consistent with the fact that H2-K^b is an integral membrane protein. These results indicate that MILL1 and MILL2 are GPI-anchored cell surface proteins.

Cell surface expression of MILL molecules is TAP-independent

RMA-S is a variant derived from RMA cells (21) that lacks functional TAP molecules because of a defective TAP2 subunit (26, 27). At 37°C, classical class I molecules are barely expressed on the surface of RMA-S cells because empty class I molecules (class I molecules without peptides) are thermodynamically unstable. However, RMA-S cells express empty class I molecules when they are cultured at lower temperatures (28). To examine whether surface expression of MILL requires TAP, we transfected RMA-S cells with MILL expression plasmids and established stable transfectants. These cells were cultured at 25°C or 37°C and stained with the anti-FLAG or anti-H2-K^b Ab. As expected, endogenous H2-K^b molecules were expressed on RMA-S cells at the level comparable to that expressed on RMA cells when these cells were cultured at 25°C (Fig. 3, *A* and *B*, *left panel*, open histograms). However, expression of H2-K^b on RMA-S cells was reduced markedly when the cells were cultured at 37°C (Fig. 3, *A* and *B*, *left panel*, shaded histograms). By contrast, the expression levels of MILL1 and MILL2 detected by the anti-FLAG Ab were nearly the same regardless of whether the RMA-S cells were cultured at 25°C or 37°C (Fig. 3, *A* and *B*, *right panel*). These results indicate that cell surface expression of MILL molecules is TAP-independent.

Cell surface-expressed MILL1 and MILL2 molecules are associated with β_2m

To examine whether MILL molecules are associated with β_2m in vivo, we performed coimmunoprecipitation analysis. After treatment of RMA-MILL1 and RMA-MILL2 cells with PI-PLC, the MILL molecules released into the supernatants were immunoprecipitated with the anti-FLAG Ab and subjected to immunoblotting analysis using the anti-FLAG and anti-mouse β_2m Ab (Fig. 4). We found that β_2m was coimmunoprecipitated with both MILL1 and MILL2, indicating that MILL molecules are associated with β_2m on the cell surface.

β_2m facilitates the refolding of MILL molecules

To examine whether MILL1 and MILL2 can associate with β_2m in vitro, we expressed the extracellular domains of MILL1 and MILL2 in *E. coli* and refolded them in the presence or absence of mouse β_2m. MILL1 could be successfully refolded only in the presence of β_2m (Fig. 5*A*, *top panel*), and MILL1 and β_2m were eluted in the same fractions in gel filtration chromatography as revealed by SDS-PAGE analysis (Fig. 5*B*, *bottom half*, *top panel*). Although MILL2 was able to form soluble proteins when it was refolded in the absence of β_2m, β_2m appeared to improve the efficacy of refolding, consistent with our other results (Fig. 5*A*, *bottom panel*). MILL2 refolded in the presence of β_2m was eluted earlier in gel filtration chromatography than that refolded in the absence of β_2m (Fig. 5*A*, *bottom panel*), indicating that MILL2

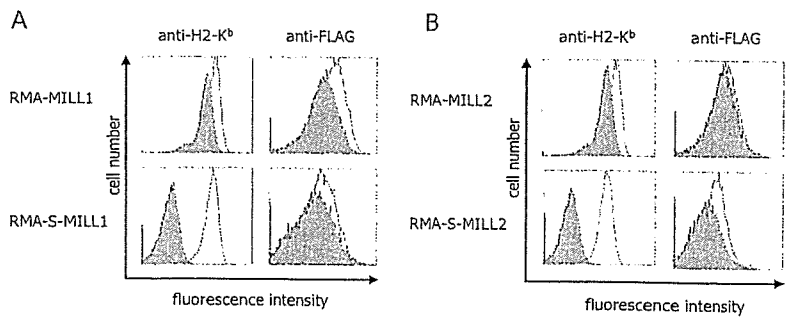

FIGURE 3. Cell surface expression of MILL molecules does not require functional TAP molecules. *A*, RMA-MILL1 and RMA-S-MILL1 cells were cultured at 25°C (open histograms) or 37°C (shaded histograms) for 18 h. Cells were incubated with anti-H2-K^b (left) or anti-FLAG (right) and then treated with FITC-conjugated F(ab')$_2$ fragments of goat anti-mouse IgG. Stained cells were analyzed by flow cytometry. *B*, RMA-MILL2 and RMA-S-MILL2 cells were treated in the same manner as in *A*, and cell surface expression of MILL2 was monitored by flow cytometry.

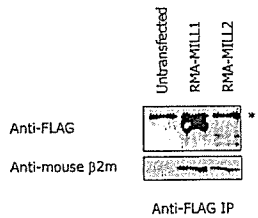

FIGURE 4. Cell surface-expressed MILL1 and MILL2 molecules are associated with β_2m. RMA-MILL1 and RMA-MILL2 cells were treated with PI-PLC and soluble MILL proteins were purified by immunoprecipitation with anti-FLAG mAb-coupled protein G-Sepharose beads (right). Precipitated samples were separated on 12% (top) or 14% (bottom) SDS-PAGE and subjected to immunoblotting analysis. MILL1 and MILL2 were detected by anti-FLAG mAb (top) whereas mouse β_2m was detected by anti-mouse β_2m Ab (bottom). Signals were detected by HRP-conjugated secondary Ab using the Super Signal West Dura kit. An asterisk indicates mouse IgG H chains.

molecules refolded in the presence of β_2m were associated with β_2m, which was further confirmed by SDS-PAGE analysis (Fig. 5*B*, *bottom panel*). MILL1 and MILL2 refolded in the presence of β_2m were purified by anion-exchange chromatography followed by gel filtration chromatography. The purified MILL1 and MILL2 proteins contained β_2m as a subunit (Fig. 5*C*). These results indicate that efficient refolding of MILL1 and MILL2 requires β_2m as a subunit. The molecular masses of MILL1/β_2m and MILL2/β_2m complexes estimated by gel filtration chromatography (Fig. 5*A*) and the relative intensities (3:1) of the MILL1 and MILL2 bands to the β_2m bands in the purified MILL1/β_2m and MILL2/β_2m complexes (Fig. 5*C*) indicate that the MILL1 or MILL2 polypeptide and β_2m bind at a 1:1 ratio.

MILL1 is expressed in a subpopulation of thymic medullary epithelial cells and a restricted region of inner root sheaths in hair follicles

To determine the tissue distribution of MILL1 and MILL2 molecules, we first performed Western blot analysis using the antisera for MILL1 and MILL2 against a panel of tissues isolated from adult and neonatal mice. These experiments yielded no bands in any tissues, presumably because the expression levels of MILL1 and MILL2 are low (data not shown). Our previous RT-PCR analysis (19) indicated that *Mill1* was transcribed in selected tissues including neonatal thymus and skin. We therefore examined expression of MILL1 in these tissues (Fig. 6). Staining was observed in a subpopulation of medullary epithelial cells in the neonatal thymus (Fig. 6*A*). These MILL1-positive cells were also detectable in the thymus of adult mice (data not shown). In the skin of 3-day-old mice, cells stained with the anti-MILL1 antiserum were found in the hair follicle (Fig. 6*B*, left). However, these cells became undetectable in the skin of 10-day-old (Fig. 6*B*, right) or 6-wk-old (not shown) mice. To more precisely address the locations of cells stained with the anti-MILL1 antiserum, we performed immunohistochemical staining of hair shafts and outer root sheaths (Fig. 6*C*). Cells stained with the anti-MILL1 antiserum were located outside the hair shaft (stained green with AE13 mAb), but inside the outer root sheath (stained green with AE1/AE3 mAb). Thus, positively stained cells are located in the inner root sheath. Because not all regions of inner root sheaths were stained with the antiserum, MILL1 seems to be expressed in a restricted region of the inner root sheath. To confirm the specificity of staining, we prepared anti-MILL1 antiserum preabsorbed with RMA-MILL1 or RMA cells. Preabsorption of the antiserum with RMA-MILL1 cells almost eliminated staining in thymic epithelial cells and hair follicles whereas staining was retained when the antiserum was preabsorbed with RMA cells (data not shown). *Mill2* is transcribed almost ubiquitously at low levels (19). We stained several tissues including neonatal thymus and skin as well as adult aorta, uterus, heart, kidney and spleen with the antiserum for MILL2 (1/200 dilution). Although this antiserum, when used at this dilution, was capable of staining RMA-MILL2 cells grown in vivo in C57BL/6 mice, we were unable to obtain any positive staining for MILL2 in any of the tissues (data not shown).

Cell surface expression of MILL1 on thymic epithelial cells requires β_2m

To examine whether cell surface expression of MILL1 requires β_2m, we isolated thymic stromal cells from 4-wk-old β_2m-deficient mice and stained with the anti-MILL1 antiserum (Fig. 7). Cell surface expression of MILL1 was almost completely abrogated in the β_2m-deficient mice compared with the adult C57BL/6 mice, indicating that cell surface expression of MILL1 is β_2m-dependent.

Discussion

MILL is the latest addition to the growing list of mammalian MHC class I families encoded outside the MHC region. Our previous work has revealed several unique features of this class I family (19, 20). First, not all mammalian species have the MILL family; although mice and rats have this family, it is absent in humans. Because MILL apparently arose before the radiation of mammals, humans seem to have lost this class I family. Second, unlike all other class I genes, the genes coding for mouse MILL have an exon between those coding for the signal peptide and the α1 domain. Third, the MILL family is phylogenetically most closely related to the MICA/B family among known class I families. Because the MILL family is absent in humans, and conversely, mice and rats lack the MICA/B family, we suggested that MILL might serve as a functional substitute of MICA/B in rodents (19). Fourth, deduced MILL molecules lack most of the residues required for the docking of peptide termini, suggesting that they are unlikely to bind peptides. Fifth, RT-PCR analysis indicated that the members of the MILL family are poorly transcribed in most adult tissues, suggesting a role other than conventional Ag presentation. Sixth, sequence comparison of rat and mouse MILL molecules revealed that *Mill* is one of the most rapidly evolving class I gene families, and that, in both *Mill1* and *Mill2*, non-synonymous substitutions occur more frequently than synonymous substitutions in the α1 domain whereas the opposite is the case in the α2 and α3 domains, suggesting that the α1 domain may be under positive selection (20). Taking all of these points into consideration, we suggested that MILL may perform specialized immune functions required only in certain species or some redundant functions, part of which are executed by other molecules (20).

In the present study, we set out to perform a biochemical characterization of mouse MILL molecules. Consistent with the absence of key residues required for the docking of peptides, we found that cell surface expression of MILL1 and MILL2 does not require functional TAP molecules (Fig. 3). Furthermore, the extracellular domains of MILL1 and MILL2 expressed in *E. coli* could be efficiently refolded in the absence of peptides under standard class I refolding conditions when β_2m was added into the mixture (Fig. 5). This is in contrast to the fact that refolding of recombinant class Ia molecules isolated from purified bacterial inclusion bodies requires the presence of a peptide ligand and is reminiscent of the behaviors of certain class Ib molecules, the refolding of which is ligand-independent (29–31). Taken together, it

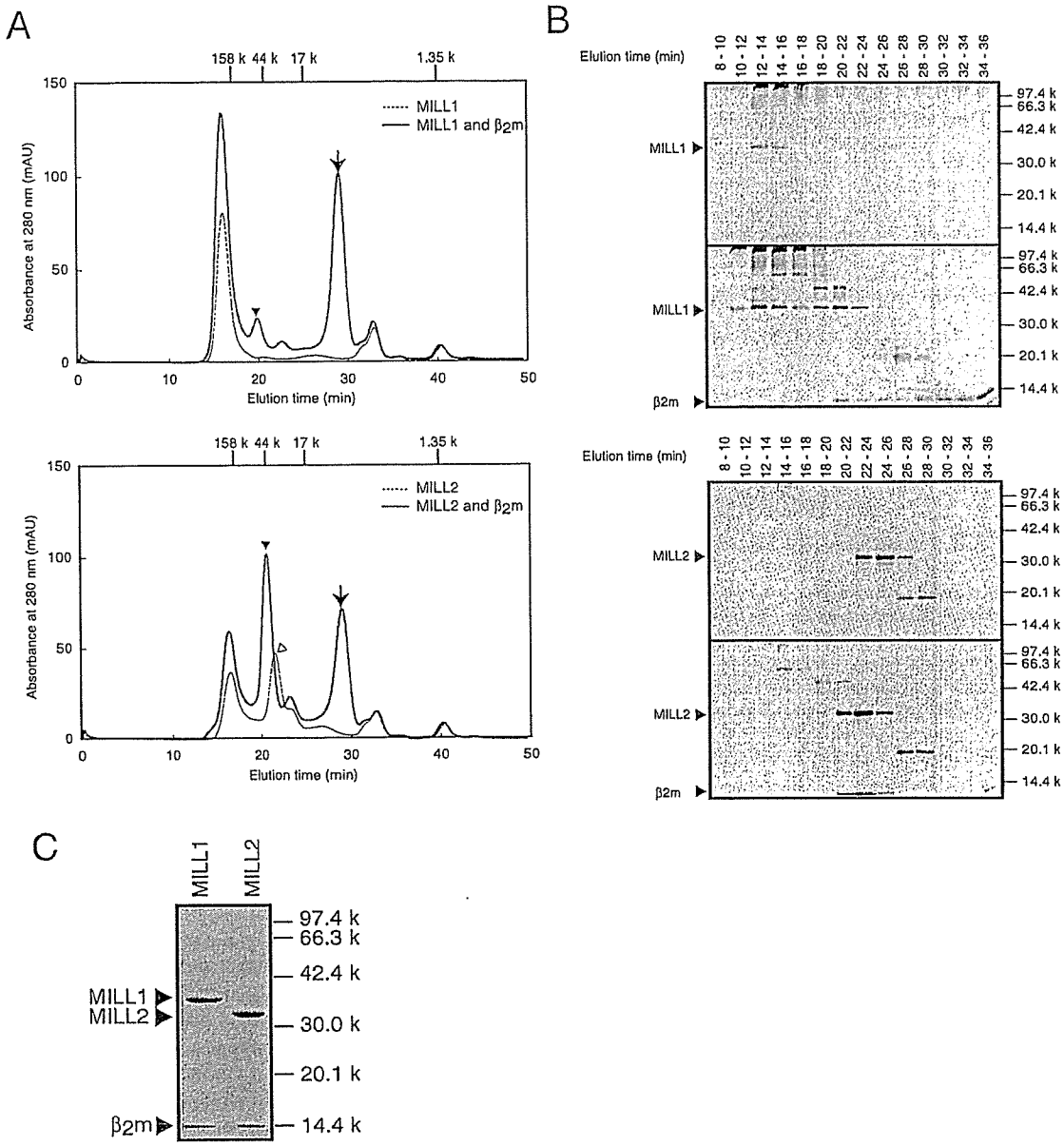

FIGURE 5. Refolding of MILL1 and MILL2 requires β_2m. *A*, Bacterially expressed extracellular domains (α1–α3) of MILL1 and MILL2 were refolded in the presence (continuous line) or absence (broken line) of β_2m and subjected to gel filtration chromatography on Superdex-75. Filled arrowheads indicate the peaks of MILL1 and MILL2 proteins associated with β_2m. Arrows indicate the peaks of free β_2m. An open arrowhead indicates the peak of MILL2 refolded in the absence of β_2m. *B*, The fractions from gel filtration chromatography were analyzed on SDS-PAGE, and the gels were stained with silver staining. The top and bottom halves of each panel indicate fractionation of the samples refolded in the absence and presence of β_2m, respectively. *C*, Coomassie brilliant blue-stained SDS-PAGE gel of in vitro refolded MILL1 and MILL2 molecules purified by sequential chromatography.

is likely that the MILL family of class I molecules performs functions other than the presentation of peptides.

Two observations made in this work were rather unexpected. First, we initially assumed that, like most other class I family members, MILL1 and MILL2 were integral membrane proteins with a transmembrane region (19, 20). Contrary to this assumption, MILL1 and MILL2 turned out to be GPI-anchored proteins (Fig. 2). The occurrence of GPI anchors is not unprecedented for class I molecules because most if not all members of RAE-1 and ULBP families as well as a large proportion of Qa-2 molecules are GPI-anchored (32–35). Like other GPI-anchored proteins (36, 37), MILL may be primarily located in lipid rafts. Second, we assumed that MILL1 and MILL2 were unlikely to be associated with β_2m because they lack many of the residues known to interact with β_2m in classical class I molecules (19). Our present work demonstrates that both MILL1 and MILL2 are associated with β_2m on the cell surface (Fig. 4). A similar unexpected association with β_2m was previously observed for MR1; this class Ib molecule lacks many of the phylogenetically conserved motifs implicated in β_2m association in class Ia molecules (38), yet biochemical studies have revealed that it associates with β_2m (38, 39). We also found that β_2m promoted refolding of bacterially produced MILL ectodomains in vitro (Fig. 5). Hence, β_2m appears to constitute an integral component of MILL class I molecules. Consistent with this, cell surface expression of MILL1 on thymic stromal cells was almost completely abrogated in β_2m-deficient mice, indicating that cell

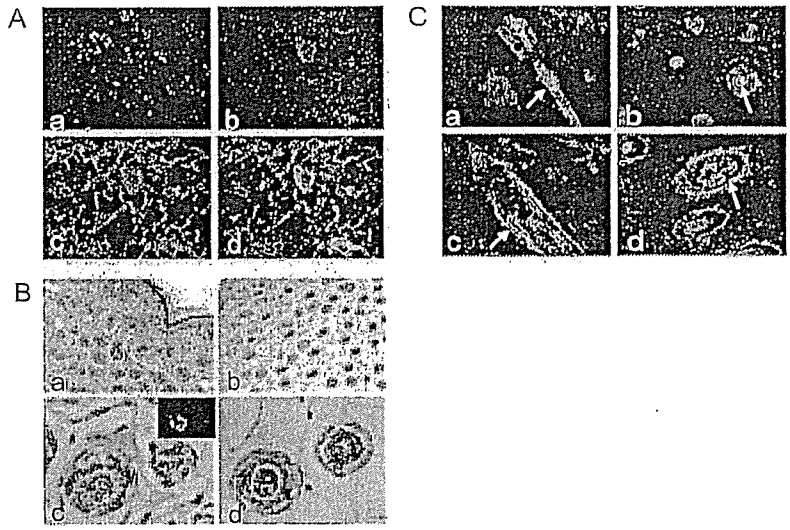

FIGURE 6. MILL1 is likely expressed in thymic medullary epithelial cells and hair follicles. *A*, Thymic tissue sections obtained from 3-day-old mice were blocked by incubation with normal goat serum (1/500 dilution), reacted with AE1/AE3 and anti-MILL1 (1/400 dilution) followed by staining with Alexa Fluor 488-conjugated goat anti-mouse IgG (1/300 dilution) and Alexa Fluor 594-conjugated goat anti-rabbit IgG (1/300 dilution). *Aa*, a low-power photo micrograph of the thymic medulla (original magnification ×100); *Ab–Ad*, a high-power magnification (original magnification ×400). Images for MILL1 (stained red, *Ab*) and AE1/AE3 (stained green, *Ac*) as well as the merged image (*Ad*) were obtained with a Nikon ECLIPSE E600 microscope. *B*, Skin tissues of 3-day-old (*Ba* and *Bc*) and 10-day-old (*Bb* and *Bd*) mice. *Upper panels*, H&E (original magnification ×100). *Lower panels*, H&E (original magnification ×400). The inset in *Bc* shows staining with the anti-MILL1 antiserum (original magnification ×100). Staining was done as described in the legend to *C*. *C*, MILL1 is likely expressed in cells of the inner root sheaths. In *Ca* and *Cb*, tissue sections were blocked by incubation with normal goat serum (1/500 dilution), reacted with AE13 (1/1000 dilution) and anti-MILL1 (1/400 dilution) and stained with Alexa Fluor 488-conjugated goat anti-mouse IgG (1/300 dilution) and Alexa Fluor 594-conjugated goat anti-rabbit IgG (1:300 dilution). In *Cc* and *Cd*, AE13 was substituted by AE1/AE3. MILL1 is stained red. The hair cortex (*Ca* and *Cb*) and outer root sheaths (*Cc* and *Cd*) are stained green. In *Ca* and *Cc*, hair shafts were sectioned parallel to the long axis. *Cb* and *Cd* show cross sections of hair shafts. Arrows in *Ca* and *Cb* indicate the hair cortex, whereas those in *Cc* and *Cd* indicate outer root sheaths. Original magnification ×400.

surface expression of MILL1 requires β_2m (Fig. 7). Given the overall structural similarity of MILL1 and MILL2 (19), and their shared biochemical properties (Figs. 2–5), it seems reasonable to assume that MILL2 also requires β_2m for cell surface expression. Because the refolding experiments showed that MILL2, but not MILL1, was able to form soluble proteins in the absence of β_2m, albeit much less efficiently than in the presence of β_2m (Fig. 5), β_2m might not be an absolute requirement for cell surface expression of MILL2. Human CD1d molecules, normally associated with β_2m, can be expressed on the surface of intestinal epithelial cells in a β_2m-independent manner (40, 41), indicating that the requirement for β_2m can differ depending on tissues. Therefore, it will be necessary to identify cells or tissues where MILL2 is physiologically expressed to determine whether cell surface expression of MILL2 requires β_2m in vivo, and if it does, whether β_2m is absolutely required.

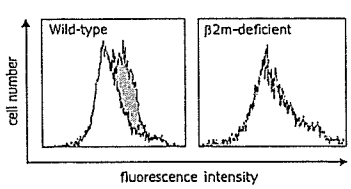

FIGURE 7. Cell surface expression of MILL1 requires β_2m. Thymic stromal cells isolated from C57BL/6 (*left panel*) and β_2m-deficient (*right panel*) mice were stained with normal rabbit serum (open histograms) or the rabbit anti-MILL1 antiserum (shaded histograms). An FITC-labeled swine anti-rabbit Ig was used as a secondary Ab. Stained cells were analyzed by flow cytometry.

Immunohistochemical analysis showed that MILL1 is expressed in a subpopulation of thymic medullary epithelial cells and a restricted region of inner root sheaths in hair follicles (Fig. 6). Expression in the thymus is suggestive of an immunological role for MILL1. Totally unexpected was the observation that some inner root sheath cells in 3-day-old, but not 10-day-old or 6-wk-old, mice were stained with the antiserum for MILL1, although we cannot rule out the possibility that our anti-MILL1 antiserum cross-reacts with epitopes on unrelated molecules in hair follicles. Hair follicles have been proposed to enjoy immune privilege (42, 43). Thus, MILL1 may somehow be involved in the establishment and maintenance of immune privilege in hair follicles. On the other hand, we have thus far been unable to identify cells expressing MILL2 proteins despite the fact that the *Mill2* gene is ubiquitously transcribed at low levels. Thus, expression of MILL2 proteins might be translationally regulated or MILL2 proteins might be expressed at detectable levels only in highly specialized cells as recently demonstrated for certain class I molecules (16, 17). It is also possible that expression of the MILL family is enhanced by certain stimuli or under pathologic conditions. To fully understand the expression patterns of the MILL family, more detailed analysis is required.

In conclusion, this study highlights the biochemical differences between the MILL and MICA/B families of class I molecules. MILL1 and MILL2 are TAP-independent, β_2m-associated glycoproteins attached to the cell surface by GPI anchors. In contrast, MICA and MICB are TAP-independent, transmembrane proteins that do not associate with β_2m (44). These two families of class I molecules also differ in their expression patterns. MICA and MICB are stress-inducible class I molecules usually not expressed

on the surface of normal cells (44). In contrast, expression of *Mill1* or *Mill2* mRNA is not inducible by heat shock (our unpublished observation), and the expression in hair follicles seems unique to the MILL family. Furthermore, our preliminary work indicates that NK cells are not stained with MILL tetramers. All of these observations argue against the possibility that MILL is a functional substitute of MICA/B in rodents. Generation of knockout mice may provide a clue for understanding the biologic function of the MILL family.

Acknowledgments

We gratefully acknowledge Dr. Taeko Nagata and Kaori Kuno for technical assistance.

Disclosures

The authors have no financial conflict of interest.

References

1. Bjorkman, P. J., and P. Parham. 1990. Structure, function, and diversity of class I major histocompatibility complex molecules. *Annu. Rev. Biochem.* 59: 253–288.
2. Klein, J. 1986. *Natural History of the Major Histocompatibility Complex.* John Wiley & Sons, New York.
3. Klein, J., and C. O'hUigin. 1994. The conundrum of nonclassical major histocompatibility complex genes. *Proc. Natl. Acad. Sci. USA* 91: 6251–6252.
4. Rodgers, J. R., and R. G. Cook. 2005. MHC class Ib molecules bridge innate and acquired immunity. *Nat. Rev. Immunol.* 5: 459–471.
5. Radosavljevic, M., and S. Bahram. 2003. In vivo immunogenetics: from *MIC* to *RAET1* loci. *Immunogenetics* 55: 1–9.
6. Bahram, S., M. Bresnahan, D. E. Geraghty, and T. Spies. 1994. A second lineage of mammalian major histocompatibility complex class I genes. *Proc. Natl. Acad. Sci. USA* 91: 6259–6263.
7. Araki, T., F. Gejyo, K. Takagaki, H. Haupt, H. G. Schwick, W. Buergi, T. Marti, J. Schaller, E. Rickli, R. Brossmer, et al. 1988. Complete amino acid sequence of human plasma Zn-α2-glycoprotein and its homology to histocompatibility antigens. *Proc. Natl. Acad. Sci. USA* 85: 679–683.
8. Fukudome, K., and C. T. Esmon. 1994. Identification, cloning, and regulation of a novel endothelial cell protein C/activated protein C receptor. *J. Biol. Chem.* 269: 26486–26491.
9. Zou, Z., M. Nomura, Y. Takihara, T. Yasunaga, and K. Shimada. 1996. Isolation and characterization of retinoic acid-inducible cDNA clones in F9 cells: a novel cDNA family encodes cell surface proteins sharing partial homology with MHC class I molecules. *J. Biochem.* 119: 319–328.
10. Fischer Lindahl, K., E. Hermel, B. E. Loveland, and C. R. Wang. 1991. Maternally transmitted antigen of mice: a model transplantation antigen. *Annu. Rev. Immunol.* 9: 351–372.
11. Treiner, E., L. Duban, S. Bahram, M. Radosavljevic, V. Wanner, F. Tilloy, P. Affaticati, S. Gilfillan, and O. Lantz. 2003. Selection of evolutionarily conserved mucosal-associated invariant T cells by MR1. *Nature* 422: 164–169.
12. Vincent, M. S., J. E. Gumperz, and M. B. Brenner. 2003. Understanding the function of CD1-restricted T cells. *Nat. Immunol.* 4: 517–523.
13. Bahram, S. 2000. MIC genes: from genetics to biology. *Adv. Immunol.* 76: 1–60.
14. Cerwenka, A., and L. L. Lanier. 2001. Natural killer cells, viruses and cancer. *Nat. Rev. Immunol.* 1: 41–49.
15. Simister, N. E., and K. E. Mostov. 1989. An Fc receptor structurally related to MHC class I antigens. *Nature* 337: 184–187.
16. Ishii, T., J. Hirota, and P. Mombaerts. 2003. Combinatorial coexpression of neural and immune multigene families in mouse vomeronasal sensory neurons. *Curr. Biol.* 13: 394–400.
17. Loconto, J., F. Papes, E. Chang, L. Stowers, E. P. Jones, T. Takada, A. Kumanovics, K. Fischer Lindahl, and C. Dulac. 2003. Functional expression of murine V2R pheromone receptors involves selective association with the M10 and M1 families of MHC class Ib molecules. *Cell* 112: 607–618.
18. Todorov, P. T., T. M. McDevitt, D. J. Meyer, H. Ueyama, I. Ohkubo, and M. J. Tisdale. 1998. Purification and characterization of a tumor lipid-mobilizing factor. *Cancer Res.* 58: 2353–2358.
19. Kasahara, M., Y. Watanabe, M. Sumasu, and T. Nagata. 2002. A family of MHC class I-like genes located in the vicinity of the mouse leukocyte receptor complex. *Proc. Natl. Acad. Sci. USA* 99: 13687–13692.
20. Watanabe, Y., T. Maruoka, L. Walter, and M. Kasahara. 2004. Comparative genomics of the *Mill* family: a rapidly evolving MHC class I gene family. *Eur. J. Immunol.* 34: 1597–1607.
21. Karre, K., H. G. Ljunggren, G. Piontek, and R. Kiessling. 1986. Selective rejection of H-2-deficient lymphoma variants suggests alternative immune defence strategy. *Nature* 319: 675–678.
22. Wada, H., N. Matsumoto, K. Maenaka, K. Suzuki, and K. Yamamoto. 2004. The inhibitory NK cell receptor CD94/NKG2A and the activating receptor CD94/NKG2C bind the top of HLA-E through mostly shared but partly distinct sets of HLA-E residues. *Eur. J. Immunol.* 34: 81–90.
23. Baba, T., A. Ishizu, H. Ikeda, Y. Miyatake, T. Tsuji, A. Suzuki, U. Tomaru, and T. Yoshiki. 2005. Chronic graft-versus-host disease-like autoimmune disorders spontaneously occurred in rats with neonatal thymus atrophy. *Eur. J. Immunol.* 35: 1731–1740.
24. Gray, D. H., A. P. Chidgey, and R. L. Boyd. 2002. Analysis of thymic stromal cell populations using flow cytometry. *J. Immunol. Methods* 260: 15–28.
25. Eisenhaber, B., P. Bork, and F. Eisenhaber. 1999. Prediction of potential GPI-modification sites in proprotein sequences. *J. Mol. Biol.* 292: 741–758.
26. Attaya, M., S. Jameson, C. K. Martinez, E. Hermel, C. Aldrich, J. Forman, K. F. Lindahl, M. J. Bevan, and J. J. Monaco. 1992. Ham-2 corrects the class I antigen-processing defect in RMA-S cells. *Nature* 355: 647–649.
27. Yang, Y., K. Fruh, J. Chambers, J. B. Waters, L. Wu, T. Spies, and P. A. Peterson. 1992. Major histocompatibility complex (MHC)-encoded HAM2 is necessary for antigenic peptide loading onto class I MHC molecules. *J. Biol. Chem.* 267: 11669–11672.
28. Ljunggren, H. G., N. J. Stam, C. Ohlen, J. J. Neefjes, P. Hoglund, M. T. Heemels, J. Bastin, T. N. Schumacher, A. Townsend, K. Karre, et al. 1990. Empty MHC class I molecules come out in the cold. *Nature* 346: 476–480.
29. Li, P., G. McDermott, and R. K. Strong. 2002. Crystal structures of RAE-1β and its complex with the activating immunoreceptor NKG2D. *Immunity* 16: 77–86.
30. Steinle, A., P. Li, D. L. Morris, V. Groh, L. L. Lanier, R. K. Strong, and T. Spies. 2001. Interactions of human NKG2D with its ligands MICA, MICB, and homologs of the mouse RAE-1 protein family. *Immunogenetics* 53: 279–287.
31. Wingren, C., M. P. Crowley, M. Degano, Y. Chien, and I. A. Wilson. 2000. Crystal structure of a γδ T cell receptor ligand T22: a truncated MHC-like fold. *Science* 287: 310–314.
32. Nomura, M., Z. Zou, T. Joh, Y. Takihara, Y. Matsuda, and K. Shimada. 1996. Genomic structures and characterization of Rae1 family members encoding GPI-anchored cell surface proteins and expressed predominantly in embryonic mouse brain. *J. Biochem.* 120: 987–995.
33. Stiernberg, J., M. G. Low, L. Flaherty, and P. W. Kincade. 1987. Removal of lymphocyte surface molecules with phosphatidylinositol-specific phospholipase C: effects on mitogen responses and evidence that ThB and certain Qa antigens are membrane-anchored via phosphatidylinositol. *J. Immunol.* 138: 3877–3884.
34. Cerwenka, A., A. B. Bakker, T. McClanahan, J. Wagner, J. Wu, J. H. Phillips, and L. L. Lanier. 2000. Retinoic acid early inducible genes define a ligand family for the activating NKG2D receptor in mice. *Immunity* 12: 721–727.
35. Cosman, D., J. Mullberg, W. Chin, R. Armitage, W. Fanslow, M. Kubin, and N. J. Chalupny. 2001. ULBPs, novel MHC class I-related molecules, bind to CMV glycoprotein UL16 and stimulate NK cytotoxicity through the NKG2D receptor. *Immunity* 14: 123–133.
36. Horejsi, V., K. Drbal, M. Cebecauer, J. Cerny, T. Brdicka, P. Angelisova, and H. Stockinger. 1999. GPI-microdomains: a role in signalling via immunoreceptors. *Immunol. Today* 20: 356–361.
37. Pizzo, P., and A. Viola. 2004. Lipid rafts in lymphocyte activation. *Microbes Infect.* 6: 686–692.
38. Miley, M. J., S. M. Truscott, Y. Y. Yu, S. Gilfillan, D. H. Fremont, T. H. Hansen, and L. Lybarger. 2003. Biochemical features of the MHC-related protein 1 consistent with an immunological function. *J. Immunol.* 170: 6090–6098.
39. Yamaguchi, H., and K. Hashimoto. 2002. Association of MR1 protein, an MHC class I-related molecule, with β_2-microglobulin. *Biochem. Biophys. Res. Commun.* 290: 722–729.
40. Balk, S. P., S. Burke, J. E. Polischuk, M. E. Frantz, L. Yang, S. Porcelli, S. P. Colgan, and R. S. Blumberg. 1994. β_2-microglobulin-independent MHC class Ib molecule expressed by human intestinal epithelium. *Science* 265: 259–262.
41. Somnay-Wadgaonkar, K., A. Nusrat, H. S. Kim, W. P. Canchis, S. P. Balk, S. P. Colgan, and R. S. Blumberg. 1999. Immunolocalization of CD1d in human intestinal epithelial cells and identification of a β_2-microglobulin-associated form. *Int. Immunol.* 11: 383–392.
42. Niederkorn, J. Y. 2003. Mechanisms of immune privilege in the eye and hair follicle. *J. Investig. Dermatol. Symp. Proc.* 8: 168–172.
43. Paus, R., B. J. Nickoloff, and T. Ito. 2005. A 'hairy' privilege. *Trends Immunol.* 26: 32–40.
44. Groh, V., S. Bahram, S. Bauer, A. Herman, M. Beauchamp, and T. Spies. 1996. Cell stress-regulated human major histocompatibility complex class I gene expressed in gastrointestinal epithelium. *Proc. Natl. Acad. Sci. USA* 93: 12445–12450.

$CD4^+/CD8^+$ macrophages infiltrating at inflammatory sites: a population of monocytes/macrophages with a cytotoxic phenotype

Tomohisa Baba, Akihiro Ishizu, Sari Iwasaki, Akira Suzuki, Utano Tomaru, Hitoshi Ikeda, Takashi Yoshiki, and Masanori Kasahara

We found a population of nonlymphoid cells expressing both CD4 and CD8 in peripheral blood mononuclear cells (PBMCs) of human T-cell leukemia virus type-I *pX* transgenic rats with autoimmune diseases. These cells, which showed a monocytic phenotype, were also found in wild-type rats, and their number increased by adjuvant-assisted immunization. GM-CSF increased the number of these double-positive (DP) monocytes in PBMCs. Consistent with the idea that DP monocytes differentiate into DP macrophages at sites of inflammation, we found infiltration of DP macrophages at the site of myosin-induced myocarditis in wild-type rats; these cells exhibited a T-helper 1 (Th1)–type cytokine/chemokine profile and expressed high levels of Fas ligand, perforin, granzyme B, and NKR-P2 (rat orthologue of human NKG2D). Adoptive transfer of GFP-positive spleen cells confirmed hematogenous origin of DP macrophages. DP monocytes had a cytotoxic phenotype similar to DP macrophages, indicating that this phenotypic specialization occurred before entry into a tissue. In line with this, DP monocytes killed tumor cells in vitro. Combined evidence indicates that certain inflammatory stimuli that induce GM-CSF trigger the expansion of a population of DP monocytes with a cytotoxic phenotype and that these cells differentiate into macrophages at inflammatory sites. Interestingly, human PBMCs also contain DP monocytes. (Blood. 2006;107:2004-2012)

Introduction

Despite their origin from a common bone marrow progenitor population, cells of the monocyte/macrophage lineage display considerable phenotypic and functional heterogeneity. Thus, macrophages residing in the liver and the lungs differ in their basal activity as well as their ability to respond to inflammatory mediators. Even within a single organ, macrophages are heterogeneous; macrophages localized in the centrilobular and periportal regions of the liver differ in size, the ability to produce superoxide anion, and phagocytic activities.[1] In an inflammatory response, the early stages are dominated by macrophages showing inflammatory and tissue-destructive activities, and, in the late stages, macrophages with tissue-restructuring activities predominate.[2] In tumor tissues, infiltrating macrophages tend to acquire a polarized M2 phenotype, promoting tumor growth and progression.[3] Accumulated evidence indicates that such macrophage heterogeneity is largely attributable to microenvironmental signals including cytokines and microbial products. Although this suggests that macrophages do not have stable, lineage-defined subsets and that their functional phenotypes change in response to a microenvironment, definitions of macrophage subpopulations are important not only for understanding their role in host defense and disease pathogenesis but also for designing effective therapeutic interventions.

In our previous study, we made F1 rats by mating F344 transgenic rats expressing the human T-cell leukemia virus type-I (HTLV-I) *pX* gene[4] to nontransgenic Wistar rats and found that they developed disorders, including atrophy of the thymus, lymphocytopenia, and inflammatory cell infiltration into multiple organs, as typically seen in chronic graft-versus-host disease (GVHD).[5] In these rats (hereafter referred to as FW-pX rats), the HTLV-I *pX* transgene induced neonatal apoptosis of the thymic epithelial cells, resulting in lymphocytopenia accompanied by compensatory expansion of peripheral myeloid cells, production of autoreactive T cells, and subsequent development of chronic GVHD-like autoimmune diseases.

In the present study, we found that a population of monocytic cells expressing both CD4 and CD8 was expanded in the peripheral blood of FW-pX rats. Monocytes/macrophages constitutively express CD4 in humans and rats[6,7] but not in mice. On the other hand, some myeloid cells including natural killer (NK) cells, mast cells, macrophages, and dendritic cells (DCs) express CD8.[8-14] We therefore hypothesized that rat peripheral blood contains a population of monocytes expressing both CD4 and CD8 and that this population is expanded under certain activating conditions. To test this hypothesis, we used a rat model of myosin-induced myocarditis. Here we show that the number of CD4/CD8 double-positive (DP) monocytes is indeed increased by adjuvant-assisted immunization with myosin or by administration of adjuvants alone and that these cells express cytotoxic factors such as perforin and granzyme B and exhibit cytotoxicity against tumor cells in vitro. Approximately half of the macrophages that infiltrated the cardiac lesion expressed both CD4 and CD8; these DP macrophages, shown to be of hematogenous origin by adoptive transfer experiments, expressed Fas ligand (Fas L), perforin, and granzyme B at high levels. Thus, our present work demonstrates the existence of a distinct population of monocytes/macrophages characterized

From the Department of Pathology/Pathophysiology, Division of Pathophysiological Science, Hokkaido University Graduate School of Medicine, Sapporo, Japan.

Submitted June 16, 2005; accepted October 17, 2005. Prepublished online as *Blood* First Edition Paper, November 3, 2005; DOI 10.1182/blood-2005-06-2345.

Supported by grants from the Ministries of Education, Culture, Sports, Science, and Technology and of Health, Labor, and Welfare, of Japan.

Reprints: Akihiro Ishizu, Department of Pathology/Pathophysiology, Division of Pathophysiological Science, Hokkaido University Graduate School of Medicine, Kita-15, Nishi-7, Kita-ku, Sapporo 060-8638, Japan; e-mail: aishizu@med.hokudai.ac.jp.

The publication costs of this article were defrayed in part by page charge payment. Therefore, and solely to indicate this fact, this article is hereby marked "advertisement" in accordance with 18 U.S.C. section 1734.

by coexpression of CD4 and CD8 and by a cytotoxic phenotype. Interestingly, human peripheral blood also contains DP monocytes.

Materials and methods

Rats

FW-pX rats were obtained by mating male F344 transgenic rats expressing the HTLV-I *pX* gene without any tissue specificity (line 38)[4] to nontransgenic female Wistar rats. Offspring were screened for the *pX* transgene by genomic polymerase chain reaction (PCR) as described.[4] FW–wild-type (FW-wt) rats were obtained by mating nontransgenic male F344 rats to female Wistar rats. HTLV-I *pX* transgenic rats (line 38) were maintained at the Institute of Animal Experimentation, Hokkaido University Graduate School of Medicine. Inbred F344 and closed-colony Wistar rats were purchased from SLC (Shizuoka, Japan) and Charles River (Kanagawa, Japan), respectively. The EGFP transgenic rats that ubiquitously expressed green fluorescent protein (GFP)[15] were obtained from the YS Institute (Utsunomiya, Japan) and Tohoku University (Sendai, Japan). All experiments using rats were done according to the Guideline for the Care and Use of Laboratory Animals in Hokkaido University Graduate School of Medicine.

Human blood samples

Human blood samples were obtained from 12 healthy donors after informed consent and used for flow cytometry (FCM). None of the donors had medical histories of autoimmune diseases, recent infection, or neoplasms.

Antibodies

Murine monoclonal antibodies (Abs) used were anti–rat CD3 (IF4 for immunohistochemistry, Cedarlane, Hornby, ON, Canada; and G4.18 for FCM, Pharmingen, San Diego, CA), anti–rat CD4 (OX-35; Pharmingen), anti–rat CD8 α-chain hinge region (OX-8; Pharmingen), anti–rat CD8 α-chain immunoglobulin (Ig) V–like region (G28; Pharmingen), anti–rat CD8 β-chain (341; Pharmingen), anti–rat CD11b/c (OX-42; Pharmingen), anti–rat CD68 (ED-1; Serotec, Oxford, United Kingdom), anti–rat CD163 (ED-2; Serotec), anti–rat B cell (RLN-9D3; Serotec), anti–rat DC (OX-62; Cedarlane), and NKR-P1A (10/78; Pharmingen), as well as anti–human CD4 (M-T466; Miltenyi Biotec, Bergisch Gladbach, Germany), anti–human CD8 (HIT8a; Pharmingen), and anti–human CD14 (MφP9; Pharmingen). Polyclonal rabbit anti–Fas L (N-20) and goat anti–granzyme B (N-19) Abs were purchased from Santa Cruz Biotechnology (Santa Cruz, CA). Mouse IgG1 or IgG2 (CBL600P or CBL601P, respectively; Chemicon International, Temecula, CA) and rabbit or goat IgG (Sigma-Aldrich, St Louis, MO) served as controls.

Recombinant cytokines/chemokines

Recombinant cytokines/chemokines used were rat RANTES and GM-CSF (PEPROTECH EC, London, United Kingdom) and mouse IL-12 (R&D Systems, Minneapolis, MN) previously shown to function in rats.[16] For in vivo administration, GM-CSF (1.0 μg per 1 mL PBS) was injected intravenously into 6-week-old Wistar rats. Peripheral blood was assayed 24 hours after injection.

FCM and MACS

Peripheral blood cells were stained by the direct method without removal of serum. After reaction with Abs, erythrocytes were depleted by treatment with ammonium chloride. Expression of cell surface molecules was analyzed using FACScan (Becton Dickinson, Franklin Lakes, NJ) with CellQuest software (Becton Dickinson). Magnetic-activated cell sorting (MACS) was done using Magnetic Cell Separator (Miltenyi Biotec) as described.[17]

Phagocytosis assay

Yellow-green carboxylate-modified 1.0 μm latex beads (Sigma-Aldrich) were mixed with rat peripheral blood (1.5×10^7 beads/300 μL blood). After incubation for 2 hours at 37°C, PE-conjugated anti-CD4 (OX-35) and PerCP-conjugated anti-CD8 (OX-8) Abs were added to the mixture, followed by depletion of erythrocytes using ammonium chloride. After 3 times wash with cold PBS, $CD4^+/CD8^+$ DP cells were gated to determine uptake of the fluorescence-labeled beads using FACScan.

Immunization of rats with porcine heart myosin and induction of myocarditis

Killed tuberculosis germs were added to Freund incomplete adjuvant (Sigma-Aldrich) to reach the concentration of 100 mg/mL. Two milligrams of myosin from porcine heart (Sigma-Aldrich) were emulsified with an equal volume (200 μL) of the prepared adjuvant. The emulsion containing porcine myosin was inoculated into bilateral footpads of 3-week-old FW-wt rats (200 μL/site).

Histopathology and immunohistochemistry

Tissue samples were fixed in 10% phosphate-buffered formaldehyde and embedded in paraffin blocks. Each 4-μm section was stained with hematoxylin and eosin. For immunohistochemistry, an avidin-biotin immunoperoxidase kit (DAKO, Glostrup, Denmark) was used. After immunostaining, tissue sections were counterstained with Mayer hematoxylin (Merck, Darmstadt, Germany).

Isolation of macrophages from cardiac tissues with myocarditis

At 3 weeks after myosin immunization, the heart was extirpated and then perfused by PBS ex vivo. The cardiac tissues were cut into small pieces and digested by 0.16% collagenase type II (Worthington Biochemical Corporation, Lakewood, NJ). After removal of tissue fragments, cell suspension was incubated in a plastic dish at 37°C. One hour later, adherent cells were harvested and used as tissue-infiltrating macrophages. The purity of ED-1–positive ($CD68^+$) positive cells regarded as macrophages was 94% (data not shown).

Immunocytochemistry

Mononuclear cells separated from rat spleen using Histopaque-1083 (Sigma-Aldrich) or isolated from cardiac tissues were cultured in chamber slides (Nalge Nunc International, Roskilde, Denmark) for 1 hour. Resultant adherent cells were fixed using cold acetone for 5 minutes or 4% paraformaldehyde for 15 minutes at room temperature and then stained by the standard method (for details, see the legends of Figures 2 and 4-6). After washing with PBS, the slides were mounted in fluorescent mounting medium (DAKO). Immunofluorescence was detected using a confocal microscope (MRC-1024; BIO-RAD, Hercules, CA) or a fluorescence microscope (ECLIPSE E600; Nikon, Tokyo, Japan).

Image processing

Microscopic photographs were taken using the objective lens (40 ×/0.75 numeric aperture) in the DP70 system (Olympus, Tokyo, Japan). DP Controller software (Olympus) was used for image processing.

RT-PCR and quantitative real-time RT-PCR

Total RNAs were extracted from cells by RNeasy Mini Kit (QIAGEN, Alameda, CA) and then reverse transcribed using M-MLV reverse transcriptase (Invitrogen, Paisley, United Kingdom). PCR was performed using the cDNAs, 2 mM dNTP mix (GeneAmp dNTPMix; Applied Biosystems, Foster City, CA), *Taq* DNA polymerase kit (AmpliTaq Gold; Applied Biosystems), and primer sets for 28 cycles of 95°C 1 minute, 56°C 1 minute, and 72°C 1 minute. Quantitative real-time reverse transcription–PCR (RT-PCR) was performed using the cDNAs, QuantiTec SYBR Green PCR Kit (QIAGEN), and primer sets. Relative expression of target genes was analyzed using the ΔΔCT method.[18] The expression level of the *Gapdh* (glyceraldehyde-3-phosphate dehydrogenase) gene was used as an internal control. PCR was conducted for 40 cycles using an ABI PRISM 7000 Sequence Detector System (Applied Biosystems) with 2-step reactions